

Lower Circulating Folate Induced by a Fidgetin Intronic Variant is Associated with Reduced Congenital Heart Disease Susceptibility

Running Title: *Wang et al.; FIGN Variant Leads to Reduced CHD Susceptibility*

Dan Wang, PhD, MD^{1,2,8,*}; Feng Wang, PhD, MD^{2,*}; Kai-Hu Shi, PhD, MD^{4,5,*}; Hui Tao, MD^{4,5}; Yang Li, PhD^{1,2}; Rui Zhao, PhD^{1,2}; Han Lu, MD¹; Wenyuan Duan, PhD⁶; Bin Qiao, BS⁶; Shi-Min Zhao, PhD^{1,2,3,7}; Hongyan Wang, PhD^{1,2,3}; Jian-Yuan Zhao, PhD^{1,2,3,7}

¹Obstetrics & Gynecology Hospital of Fudan University, State Key Laboratory of Genetic Engineering, School of Life Sciences and Institutes of Biomedical Sciences, Fudan University, Shanghai, P.R. China; ²Key Laboratory of Reproduction Regulation of NPFPC, Institute of Reproduction & Development and Children's Hospital of Fudan University, Fudan University, Shanghai, P.R. China; ³MOE Key Laboratory of Contemporary Anthropology, Collaborative Innovation Center for Genetics & Development, Fudan University, Shanghai, P.R. China; ⁴Department of Cardiothoracic Surgery, Second Hospital of Anhui Medical University, Anhui Medical University, Hefei, P.R. China; ⁵Cardiovascular Research Center, Anhui Medical University, Hefei, P.R. China; ⁶Institute of Cardiovascular Disease, General Hospital of Jinan Military Region, Jinan, P.R. China; ⁷Collaborative Innovation Center for Biotherapy, West China Hospital, Sichuan University, Chengdu, P.R. China; ⁸Department of Neonatology, First Affiliated Hospital of Wenzhou Medical University, Wenzhou, P.R. China

*These authors contributed equally to this work

Addresses for Correspondence:

Shi-Min Zhao, PhD
Fudan University
Suite C321, Life Science Building
2005 Songhu Rd, Shanghai
200438, P.R. China
Tel: 86-21-51630422
Fax: 86-21-51630419
Email: zhaosm@fudan.edu.cn

Hong-Yan Wang, PhD
Fudan University
wanghy@fudan.edu.cn

Jian-Yuan Zhao, PhD
Fudan University
zhaojy@fudan.edu.cn

Journal Subject Terms: Genetic, Association Studies; Basic Science Research; Risk Factors; Congenital Heart Disease

Abstract

Background—Folate deficiency is an independent risk factor for congenital heart disease (CHD); however, the maternal plasma folate level is paradoxically not a good diagnostic marker. Genome-wide surveys have identified variants of non-folate metabolic genes associated with the plasma folate level, suggesting that these genetic polymorphisms are potential risk factors for CHD.

Methods—To examine the effects of folate concentration-related variations on CHD risk in the Han Chinese population, we performed three independent case-control studies including a total of 1,489 CHD patients and 1,745 controls. The expression of the Fidgetin (*FIGN*) was detected in human cardiovascular and decidua tissue specimens using qRT-PCR and western blotting. The molecular mechanisms were investigated by luciferase reporter assays, surface plasmon resonance, and chromatin immunoprecipitation. *FIGN*-interacting proteins were confirmed by tandem affinity purification and co-immunoprecipitation. Proteasome activity and metabolite concentrations in the folate pathway were quantified using a commercial proteasome activity assay and immunoassays, respectively.

Results—The +94762G>C (rs2119289) variant in intron 4 of the *FIGN* gene was associated with significant reduction in CHD susceptibility ($P = 5.1 \times 10^{-14}$ for the allele, $P = 8.5 \times 10^{-13}$ for the genotype). Analysis of combined samples indicated that CHD risks in individuals carrying heterozygous (GC) or homozygous (CC) genotypes were reduced by 44% (odds ratio [OR] = 0.56, 95% confidence interval [CI] = 0.47–0.67) and 66% (OR = 0.34, 95% CI = 0.23–0.50), respectively, compared to those with the major GG genotype. Minor C allele carriers who had decreased plasma folate levels exhibited significantly increased *FIGN* expression because the transcription suppressor CREB1 did not bind the alternative promoter of *FIGN* isoform X3. Mechanistically, increased *FIGN* expression led to the accumulation of both reduced folate carrier 1 (RFC1) and dihydrofolate reductase (DHFR) via inhibition of their proteasomal degradation, which promoted folate absorption and metabolism.

Conclusions—We report a previously undocumented finding that decreased circulating folate levels induced by increased folate transmembrane transport and utilization, as determined by the Fidgetin intronic variant, serves as a protective mechanism against CHD. Our results may explain why circulating folate levels do not have a good diagnostic value.

Key-Words: proteasome; congenital heart disease, folate transmembrane transport, folate utilization, Fidgetin variant

Clinical Perspective

What is new?

- In 1,489 CHD patients and 1,745 controls of the Han Chinese population, *FIGN* +94762G>C (rs2119289) intronic variant is associated with decreased circulating folate levels and increased protection against CHD.
- Increased *FIGN* expression inhibits proteasomal degradation of reduced folate carrier 1 (RFC1) and dihydrofolate reductase (DHFR).
- *FIGN* facilitates cellular uptake and metabolism of folate via upregulation of RFC1 and DHFR.
- This study demonstrates that folate utilization, rather than circulating folate levels, determines the preventive effect against CHD.



What are the clinical implications?

- A combination of circulating folate levels and folate utilization efficiency would serve as a better predictive biomarker of CHD.
- Folate utilization/metabolism is strongly regulated by *FIGN*-mediated degradation of folate metabolic enzymes, revealing a novel mechanism to enhance folate utilization by increasing *FIGN* expression.
- These findings provide new insights into the relationship of circulating folate levels with CHD and other folate-associated diseases.

Introduction

Congenital heart disease (CHD), the most common congenital human birth defect, affects 9.1 per 1,000 live births worldwide.¹ The etiology of CHD involves both genetic and environmental factors.² Epidemiological studies had found that folate deficiency is the leading cause of CHD,^{3,4} which was confirmed by multiple evidence from genetic studies regarding enzymes involved in folate metabolism. On the one hand, the core folate metabolic gene variants that attenuate folate metabolism increase the incidence of CHD. The polymorphisms in the methylenetetrahydrofolate reductase-encoding gene (*MTHFR* c.677C>T and c.1298A>C) have been associated with elevated levels of homocysteine and increased risk of CHD through reduction of enzymatic activity.⁵⁻⁸ The c.653R>Q variant of *MTHFD1*, a trifunctional cytoplasmic enzyme acting as methylenetetrahydrofolate dehydrogenase, cyclohydrolase, and formyltetrahydrofolate synthetase 1, impairs enzymatic activity and increases the risk for CHD.⁹ In our previous studies, we identified noncoding variants in the genes of methionine synthase (*MTR* -186G>T and +905G>A) and methionine synthase reductase (*MTRR* c.56+781A>C), which increase the risk of CHD through reduction of gene transcription leading to the accumulation of homocysteine.^{10,11} On the other hand, the core folate metabolic gene variants that increase the efficiency of folate metabolism reduce the risk of CHD. Our previous studies found that the promoter variant -551C>G of the cystathionine β -synthase-encoding gene (*CBS*) is associated with decreased CHD risk through activation of *CBS* transcription and subsequent stimulation of homocysteine removal.¹² The rs11254363 variant of the cubilin-encoding gene (*CUBN*) reduces the risk of CHD by increasing the level of circulating vitamin B12 which plays the key role in the

folate-dependent re-methylation of homocysteine to methionine by MTR.¹³ More importantly, periconceptional administration of folic acid protects newborns from various congenital abnormalities, including a 40–60% decrease in CHD risk,^{4,14,15} while exposure to folic acid antagonists during pregnancy increases the risk of CHD in the offsprings.¹⁶ These facts suggest that genetic polymorphisms affecting folate or homocysteine levels represent potential risk factors for CHD and other folate deficiency-related diseases.

Although folate deficiency is firmly established as a risk factor,³ the predictive value of circulating folate levels is paradoxically unsatisfactory.¹⁷⁻¹⁹ The lack of predictive value suggests that the mechanism and key factors involved in folate deficiency are not fully understood; that is, regulators involved in folate uptake and metabolism are likely yet to be identified. A genome-wide association study (GWAS) showed that the plasma folate concentration may be associated with polymorphisms in synaptotagmin 9 (*SYT9*), antisense RNA 1 of prickle planar cell polarity protein 2 (*PRICKLE2-AS1*), gamma-aminobutyric acid type B receptor subunit 2 (*GABBR2*), calcium voltage-gated channel subunit alpha1 E (*CACNA1E*), neuroblastoma breakpoint family member 3 (*NBPF3*), and fidgetin (*FIGN*).^{20,21} FIGN is an ATPase highly expressed in multiple developing organs, including the heart, and is implicated in the maintenance of normal embryonic development.²² Surprisingly, none of the newly identified folate levels regulating genes have been previously mentioned as directly involved in folate metabolism, suggesting that the panel of risk factors associated with folate deficiency-related diseases should be extended. Therefore, the investigation of non-folate metabolic enzymes such as FIGN would allow revealing



novel pathogenic mechanisms that may explain some of the current puzzling observations regarding CHD risk factors. In the current study, we examined 6 folate-related polymorphisms in three independent case-control groups comprising 1,489 CHD patients and 1,745 healthy individuals from the Han Chinese population. In particular, we investigated the molecular mechanism affected by the *FIGN* intronic variant +94762G>C which decreased plasma folate levels but showed strong protection against CHD.

Methods

Study Participants



Blood samples were obtained from three independent case-control groups including a total of 1,489 CHD patients and 1,745 healthy children as control (Supplemental Table 1): the Shanghai City, Shandong Province, and Anhui Province groups consisted of 304 and 321, 564 and 610, and 621 and 814 patients and healthy controls, respectively. In addition, 50 human cardiovascular tissue samples were used to examine *FIGN* expression, another 50 human cardiovascular tissue samples were used to measure folate concentration, and 27 human decidua and matched plasma samples were used to investigate *FIGN*-regulated folate absorption. Plasma folate and homocysteine concentrations were measured in 204 blood samples obtained from healthy fasting children. All study protocols were reviewed and approved by the ethics committees of each medical center, and written consent was obtained from parents and/or patients prior to commencing the study. The profiles of the study groups and the inclusion and exclusion criteria are described in detail in the SUPPLEMENTAL MATERIAL.

The demographic characteristics of CHD patients and healthy children, including maternal use of folic acid and maternal/paternal smoking and drinking statuses, provided in Supplemental Table 2, indicate that no significant demographic differences existed between patients and controls.

Single Nucleotide Polymorphism (SNP) Selection and Genotyping

Genetic polymorphisms listed in Supplemental Table 3 were determined by genotyping using the SNaPshot kit (ABI, Foster City, CA, USA) as described in SUPPLEMENTAL MATERIAL. All the primers used were listed in Supplemental Table 4.

Reverse Transcription, PCR, and Western Blotting

Reverse transcription, PCR, absolute/relative quantitative real-time qRT-PCR, and western blotting protocols are presented in SUPPLEMENTAL MATERIAL. All the primers used were listed in Supplemental Table 4.

Plasmid Construction, Cell Culture, and Transfection

To construct the luciferase reporter plasmid containing the *FIGN* variant, a 948-bp fragment comprising a sequence from +94,290 to +95,237 bp of *FIGN* intron 4 which contains the +94762 site was cloned into the pGL3-basic vector (Promega, Madison, WI, USA). The cDNA clones of *FIGN* and cAMP-responsive element-binding protein 1 (*CREB1*) were purchased from OriGene (Rockville, MD, USA), and those of *PSMD4*, *PSMC5*, and *PSMD13* were obtained from Dr. Jiahuai Han (<http://hanlab.xmu.edu.cn/cdna/>). Culture conditions for human embryonic kidney 293T (HEK293T) cells, rat cardiac myocytes (H9C2), and human dermal fibroblasts (HDFs), as well as plasmid construction and cell transfection are described in SUPPLEMENTAL



MATERIAL.

Surface Plasmon Resonance Analysis

The surface plasmon resonance (SPR) analysis was performed using the ProteOn XPR36 Protein Interaction Array System (Bio-Rad, Hercules, CA, USA), as described in SUPPLEMENTAL MATERIAL.

Chromatin Immunoprecipitation Assays

The chromatin immunoprecipitation (ChIP) assays were conducted using the EZ ChIP Kit (Upstate, Lake Placid, NY, USA), as described in SUPPLEMENTAL MATERIAL.

Tandem Affinity Purification

HEK293T cells were transfected with pMCB-SBP-Flag-*FIGN* containing a puromycin resistance marker. Cells stably expressing *FIGN* were lysed on ice in 0.1% NP40 buffer, centrifuged to remove insoluble cell debris, and the resulting cell lysates were incubated with streptavidin-conjugated beads for 3 h at 4°C. The precipitates were washed three times with 0.1% NP40 buffer, two times with ddH₂O, and three times with 50 mM NH₄CO₃, and subjected to tryptic digestion at 37°C overnight. The peptides in the supernatant were collected by centrifugation, dried in a speed vacuum, and re-dissolved in NH₄CO₃ buffer containing 0.1% formic acid and 5% acetonitrile for mass spectrometry analysis.

Proteasome Activity Measurement

Proteasomal activity was measured using the Proteasome Activity Assay Kit (Abcam, Cambridge, UK), as described in SUPPLEMENTAL MATERIAL.

Metabolite Quantification in Human Plasma, Tissues, and Cultured Cells



Folate concentration was detected by the Elecsys FOL III competitive chemiluminescent immunoassay (Roche, Shanghai, China) using a Cobas E411 Analyzer (Roche). Homocysteine concentration was quantified using the Axis® Homocysteine Enzyme Immunoassay (EIA) Kit (Axis-Shield, Norton, MA, USA), and S-adenosylmethionine (SAM) and S-adenosylhomocysteine (SAH) were measured using the SAM & SAH ELISA Combo Kit (Cell Biolabs, San Diego, CA, USA). Detailed information is provided in SUPPLEMENTAL MATERIAL.

DNA Synthesis and Cell Proliferation Assays

After cell transfection, DNA synthesis was measured using 5-ethynyl-2'-deoxyuridine (EDU) staining and cell proliferation was assessed using the Cell Counting Kit-8 (CCK-8) (Dojindo Laboratories, Kumamoto, Japan) as described in SUPPLEMENTAL MATERIAL.

Statistical Analysis

Differences in qualitative demographic features and allelic and genotypic frequencies between CHD patients and healthy individuals were evaluated by the χ^2 test and Fisher exact test using the SPSS 15.0 software (SPSS, Chicago, IL, USA). Deviations from the Hardy-Weinberg equilibrium in controls were examined by the χ^2 test. To determine associations between genotypes and the CHD risk, odds ratios (ORs) and 95% confidence intervals (CIs) were calculated using unconditional logistic regression analysis with adjustments for age and sex. For other parameters, differences between groups were evaluated using Student's *t*-test. All statistical tests were two-tailed, and $P < 0.05$ was considered statistically significant.

Results

***FIGN* Intronic Variant Significantly Reduces the Risk of CHD**

In the Shanghai group, the genotype distribution of only one SNP, *FIGN* +94762G>C (rs2119289) located within intron 4, was significantly different between CHD patients and healthy subjects ($P = 0.0048$). The minor C allele was associated with a reduced risk of CHD (per allele adjusted OR = 0.61, 95% CI = 0.46–0.81, $P = 0.001$) (Table 1). Similar results were observed in the Shandong group (per allele adjusted OR = 0.52, 95% CI = 0.42–0.65, $P = 7.7 \times 10^{-5}$) and in the Anhui group (per allele adjusted OR = 0.69, 95% CI = 0.58–0.82, $P = 1.3 \times 10^{-4}$) (Table 1), confirming that the *FIGN* +94762C allele indicated a decreased risk of CHD compared with the major G allele.

In healthy individuals, genotype frequencies of all polymorphisms corresponded to the Hardy-Weinberg equilibrium ($P > 0.05$; Table 1). The allelic and genotypic frequencies of the six investigated polymorphisms are listed in Supplemental Tables 3 and 5. Minor allele frequency (MAF) of each polymorphism was consistent with the data reported for the Han Chinese population in the dbSNP database (Supplemental Table 3). The maternal folic acid intake rate was not significantly different among the three *FIGN* genotypes (+94762GG, GC, and CC) in CHD patients and controls (Supplemental Table 6).

The combined data obtained from the entire analyzed population indicated that the +94762C allele was associated with a 39% decrease in the CHD risk (adjusted OR = 0.61, 95% CI = 0.54–0.69), whereas the GC genotype was associated with a 44% reduction (adjusted OR = 0.56, 95% CI = 0.47–0.67), and the CC genotype with a 66% reduction (adjusted OR = 0.34, 95% CI =

0.23–0.50) in the CHD risk compared with the major G allele or GG genotype (allele distribution $P = 5.1 \times 10^{-14}$, genotype distribution $P = 8.5 \times 10^{-13}$) (Table 1).

Stratified analysis of *FIGN* +94762G>C performed according to the CHD classification described previously¹² indicated that this SNP was significantly associated with septation defects (1,222 cases, $P = 3.84 \times 10^{-13}$) and conotruncal defects (267 cases, $P = 0.0012$). With respect to the CHD subtypes, the *FIGN* variant significantly correlated with ventricular septal defects (932 cases, $P = 1.92 \times 10^{-8}$) (Supplemental Table 7).

***FIGN* Genotype is Strongly Correlated with a Reduced Plasma Folate Concentration**

Next, we explored the relationship between *FIGN* +94762G>C and plasma folate levels in 204 fasting healthy children using the Elecsys Folate assay. The results revealed that *FIGN* +94762G>C was significantly associated with plasma folate levels in the Han Chinese population ($P = 0.01$; Figure 1a). Heterozygous or homozygous +94762C allele carriers exhibited 10.7% ($P = 0.045$) and 32.6% ($P = 0.009$) lower folate levels, respectively, compared to the major GG genotype carriers. In addition to low folate levels, carriers of +94762CC or GC also had decreased plasma homocysteine levels compared to those with the major GG genotype, although the difference was not statistically significant (Figure 1b). These results contradict the notion that folate levels are negatively correlated with homocysteine levels and the risk of CHD.

SNP +94762G>C is Associated with Increase in *FIGN* Isoform X3 Expression

We next investigated the mechanism underlying the *FIGN* +94762G>C-mediated reduction in CHD risk in the setting of a reduced plasma folate concentration. We explored whether the +94762G>C variant affects *FIGN* expression because this polymorphism is located in the

regulatory region of *FIGN*. Analysis of *FIGN* mRNA levels in 50 cardiovascular tissue samples by qRT-PCR using *FIGN* exon 7-specific primers (Figure 2a) revealed that *FIGN* transcription was increased by 45% and 83% in the samples from people with +94762GC and CC genotypes compared to those with the GG genotype (Figure 2b), suggesting the SNP effect on *FIGN* expression. However, when we used primers targeting *FIGN* exon 1, no significant differences in *FIGN* expression among the genotypes were observed (Figure 2b). This suggests that the transcription of *FIGN* was influenced by the +94762C>G variant. As shown in Figure 2a, the *FIGN* gene spans >130 kb and contains seven exons. In humans, five different *FIGN* isoforms are encoded by six alternative short exons (1 to 6). The expression patterns of the *FIGN* isoforms were investigated in human cardiovascular tissues using cross-intron primers; as a result, *FIGN* isoforms X1, X3, and X4 were detected (Figure 2c). Absolute quantification using qRT-PCR showed that X3 was the predominant isoform expressed in the heart (Figure 2d). Moreover, only X3 expression significantly depended on the *FIGN* genotype, following the same pattern observed using exon 7-specific primers. Individuals carrying the GC and CC genotypes showed 71% and 126% increases, respectively, in isoform X3 expression compared with GG carriers (Figure 2e). Since *FIGN* isoforms X3 and X1 encode the same protein, the increase in isoform X3 mRNA may correspond to that in *FIGN* protein. Therefore, we examined *FIGN* protein expression in 18 human cardiovascular tissue samples with different *FIGN* +94762G>C genotypes using western blotting. The results indicated that *FIGN* protein levels were 63% and 122% higher in tissues with GC and CC genotypes, respectively, compared to those with the major GG genotype (Figure 2f).

SNP +94762G>C Activates an Alternative Promoter within *FIGN* Intron 4

We then explored the mechanism underlying the increase in *FIGN* isoform X3 transcription in +94762C carriers. By analyzing the intronic sequence surrounding the +94762 site, we inferred that this DNA region may represent a traditional promoter because it contained five TATA boxes, which are RNA polymerase II (Pol II) binding sites, and two CAAT boxes, which are *cis*-elements of the core promoter region (Figure 2a and Supplemental Figure 1). We cloned a 948-bp fragment containing either +94762G or C in the pGL3 vector and performed luciferase assays (Figure 2a). Although both intron 4 fragments could initiate transcription in human HEK293T and rat H9C2 cells, the protective C allele provided a 2.1- and 2-fold increase in luciferase expression, respectively, compared with the G allele (Figure 3a). These results were consistent with the findings in human tissues, confirming that the intronic +94762G>C variant upregulated the transcription of *FIGN* isoform X3.

SNP +94762G>C Attenuates the Binding Affinity of Transcriptional Repressor CREB1

Computational analysis (TFBIND, <http://tfbind.hgc.jp>) predicted that *FIGN* intron 4 contained a binding motif for cAMP responsive element-binding protein 1 (CREB1) transcription factor, which was centered around the +94762 site, while the *FIGN* promoter region did not contain such motif (Supplemental Figure 1), suggesting that CREB1 may specifically regulate isoform X3 transcription. The SPR assay using purified CREB1 revealed that the binding affinity of the major +94762G allele to CREB1 was more than 1,000-fold higher than that of the minor C allele (Figure 3b). The ChIP assay performed in HEK293T cells demonstrated that the intron 4 +94762 site was occupied by CREB1 and RNA polymerase II (Pol II) (Figure 3c). ChIP analysis of

human cardiovascular tissues indicated that the CC genotype was associated with a 47% reduction in CREB1 binding and a 78% increase in Pol II binding to the +94762 site compared with the major GG genotype (Figure 3d), suggesting that CREB1 functions as a repressor of *FIGN* isoform X3 transcription. Exogenous CREB1 expression decreased the promoter activity of *FIGN* isoform X3, and the disparity in promoter function caused by the +94762G>C polymorphism was reduced (Figure 3a). Endogenous CREB1 knockdown by specific siRNA in HEK293T cells with the wild-type +94762GG genotype activated *FIGN* expression both at the mRNA and protein levels (Figure 3e).

FIGN Inhibits Cellular Proteasome Activity



Next, we explored the effects of increased *FIGN* expression on the CHD risk. We used tandem affinity purification to identify *FIGN*-interacting proteins in HEK293T cells. As a result, a total of 165 different proteins were detected in cells (Supplemental Table 8). Gene ontology analysis showed that the *FIGN*-interacting proteins were enriched for proteasome-related functions (Figure 4a and Supplemental Figure 2). Eight proteasome subunits were shown to interact with *FIGN*, including PSMD4 (Rpn10), which is the polyubiquitin receptor; PSMD3 (Rpn3), PSMD6 (Rpn7), and PSMD13 (Rpn9), which assemble the lid of the 19S regulatory particle; PSMD2 (Rpn1), PSMC3 (Rpt5), and PSMC5 (Rpt6), which are key components in the base of the 19S regulatory particle; and PSMA4 (α 3), which is a component of the α -ring in the 20S core particle (Supplemental Table 9).²³ In co-immunoprecipitation assays, we validated *FIGN* binding to PSMD4, PSMC5, and PSMD13, confirming the interaction between *FIGN* and the proteasome (Figure 4b–d). Cumulatively, these results suggest that *FIGN* regulates proteasomal function.

The levels of FIGN-interacting proteasome subunits PSMD4, PSMD13, and PSMC5 were not altered in FIGN-overexpressing cells (Figure 4e). However, a 2-fold increase in FIGN expression (the exogenous FIGN protein exhibited smaller band size because of lack of glycosylation; Supplemental Figure 3), which corresponded to FIGN upregulation in +94762CC carriers compared to major GG carriers, significantly inhibited proteasome activity in both HEK293T cells and HDFs (Figure 4f).

FIGN Increases RFC1 and DHFR Expression

Reduced folate carrier 1 (RFC1) and dihydrofolate reductase (DHFR), key proteins involved in folate metabolism, are regulated by the ubiquitin-proteasome system.^{24,25} By treating HEK293T cells with cycloheximide (CHX), we demonstrated that inhibition of translation did not prevent the degradation of RFC1 and DHFR (Figure 5a). Moreover, enhanced FIGN expression resulted in increased stability of both RFC1 and DHFR (Figure 5b), as the half-lives of these proteins in FIGN-overexpressing cells significantly increased (from 2.6 and 0.8 h to 5.9 and 2.5 h, respectively; Supplemental Figure 4a and b). At the same time, FIGN knockdown promoted the degradation of RFC1 and DHFR (Figure 5c), as evidenced by a reduction in their half-lives (from 2.9 and 1 h to 1.9 and 0.5 h, respectively; Supplemental Figure 4c and d). Furthermore, proteasomal inhibitor MG132 induced RFC1 and DHFR accumulation, indicating that both proteins were degraded via the ubiquitin-proteasome system (Figure 5d). FIGN overexpression in HEK293T cells and HDFs upregulated RFC1 and DHFR proteins but not mRNAs (Figure 5e). The increase in RFC1 and DHFR proteins induced by FIGN overexpression was saturated by MG132, confirming that FIGN modulated RFC1 and DHFR degradation via proteasome

inhibition (Figure 5f). When we activated FIGN expression using CREB1-specific siRNA, RFC1 and DHFR proteins increased significantly (Figure 5g). Positive correlation of RFC1 and DHFR protein levels with FIGN expression was validated in cardiovascular tissues with different *FIGN* genotypes. Thus, the expression of RFC1 was 38% and 85% higher, while that of DHFR was 47% and 110% higher in tissues with +94762GC and CC genotypes, respectively, compared to those with the GG genotype (Figure 2f). Taken together, these results indicated that FIGN upregulated RFC1 and DHFR expression.

Increased FIGN Levels Promote Folate Transmembrane Transport and Utilization

RFC1 and DHFR play important roles in folate absorption and utilization. We observed that in culture medium with high folate levels (1 $\mu\text{g/ml}$), a 2-fold increase of FIGN in HEK293T led to a 72% increase in intracellular folate levels (Figure 6a). In culture medium with a low folate level that close to human plasma folate concentration (10 ng/ml), enhanced FIGN expression caused a 50% increase in folate levels and, more importantly, a 35% reduction in folate levels in the culture medium (Figure 6b). This phenomenon was further confirmed in HDFs and H9C2 cells cultured with the low folate concentration (Figure 6c). These results indicate that the increased FIGN expression may promote the folate transmembrane transport. In addition, we showed that enhanced FIGN expression promoted the removal of homocysteine (an independent CHD risk factor) (Figure 6d), increased SAM and the SAM/SAH ratio (an index of methylation potential) (Figure 6e), and upregulated DNA synthesis as evidenced by EDU staining (Figure 6f). These results indicate that folate metabolism is induced by the increase in FIGN expression.

Notably, we observed that, although decreased folate concentration in culture medium

slowed HEK293T cell proliferation, FIGN overexpression restored cell growth inhibited by low folate and stimulated it even at normal folate concentration (Figure 6g). These results indicated that FIGN was important for folate utilization and cell proliferation. Therefore, we next analyzed *FIGN* expression during heart development in experimental animals and primary human cells. In mice, *Fign* transcription was higher in the E12, E16, and E20 embryonic heart (Figure 6h) compared to that in the neonatal and adult hearts, while in rats, *Fign* expression was higher in fetal hearts than in the corresponding maternal hearts both at the mRNA and protein levels (Figure 6i). Moreover, FIGN levels in proliferating chorion cells derived from human embryos were higher than those in the corresponding maternal decidua cells both at the mRNA and protein levels (Figure 6j). These observations were consistent with the notion that proliferating cells required high FIGN levels, suggesting a critical role of FIGN for cardiac embryonic development.

SNP +94762G>C Decreases Folate in Plasma while Increasing it in Tissues

Next, we wanted to confirm the observation that increased FIGN expression facilitated folate transport from the extracellular environment to the intracellular space in human samples. In human cardiovascular tissues with different *FIGN* genotypes, the +94762GC or CC genotypes were associated with higher folate content (5.9%, $P = 0.22$, and 19.7%, $P = 0.002$, respectively) compared to the GG genotype (Figure 7a). Furthermore, among healthy women who had spontaneous abortion, the +94762CC genotype carriers exhibited 35.4% lower plasma folate levels ($P = 0.0001$, Figure 7b) and 13.8% higher decidua folate levels ($P = 0.02$; Figure 7c) compared to the major GG genotype carriers. In addition, women with the +94762GC genotype

also tended to have decreased folate in plasma and increased folate levels in decidua compared to those with the major GG genotype, although the difference was not statistically significant (Figure 7b, c). In addition, individuals carrying the GC and CC genotypes displayed 57% and 104% increase in the expression of *FIGN* isoform X3, and 52% and 89% increase in total *FIGN* mRNA, respectively, compared to those with the GG genotype (Figure 7d). Consistently, *FIGN* protein expression was 51% or 110% higher in the samples with +94762GC or CC genotypes, respectively, than in those with the GG genotype (Figure 7e). These data obtained in maternal samples support a mechanistic model suggesting that the *FIGN* +94762G>C polymorphism promoted folate transport from plasma to cardiac tissue through activation of *FIGN* isoform X3 transcription.

Discussion

Limitations in the predictive value of plasma folate levels for folate deficiency-related diseases such as CHD and neural tube defect (NTD) suggest that other factors are involved in the pathology of folate deficiency.^{17-19,26} Our study provides evidence to show that genes determine folate utilization efficiency, affect CHD risk, independent of circulating folate levels. The *FIGN* +94762G>C variant we found in the center of large 55,343-bp intron 4 increases folate utilization efficiency and protects against CHD, although it decreases circulating folate levels.

The region surrounding +94762G>C represents a traditional promoter containing *cis*-regulatory elements, i.e., TATA and CAAT boxes. Our data indicate that the +94762G>C substitution eliminates the binding site for transcriptional repressor CREB1, thus promoting the

recruitment of Pol II and activating alternative transcription of *FIGN* isoform X3. This notion is supported by the finding that the expression of *FIGN* isoform X3 was dose-dependently associated with the number of +94762C alleles in human cardiac and decidua tissues (Figure 2e, 7d). Moreover, *FIGN* interacts with and inhibits proteasome activity, promoting the accumulation of RFC1 and DHFR, key factors in folate uptake and metabolism known to be degraded via the ubiquitin-proteasome pathway.^{24,25} These findings are consistent with previous reports that CREB1, the transcription suppressor of *FIGN*, is able to activate proteasome activity,^{27,28} as well as with our present data that *FIGN* upregulation in human tissues is associated with the +94762G>C polymorphism.



FIGN expression starts at mouse embryonic day E8.5,²² i.e., at the early stage of heart development.²⁹ Here, we also confirmed high expression of *Fign* mRNA in the mouse embryonic heart at E12, E16, and E20 compared to the adult organ (Figure 6h). The stages of heart looping, chamber formation, and ventricular/atrial/outflow tract septation are initiated in the embryo at E9, E10, and E11–E15, respectively,²⁹ and *FIGN* is involved in the initiation and progression of these processes by promoting folate transport and utilization. As expected, our association analysis has shown that the *FIGN* +94762C allele is associated with a reduced risk for congenital ventricular septal and atrial septal defects, and Tetralogy of Fallot (Supplemental Table 7). These findings revealed a previously unreported pathway of *FIGN*-mediated regulation of folate metabolism and indicated that embryonic stage-dependent inhibition of proteasome activity is essential for the initiation of early prenatal development. Furthermore, in the early stage of embryogenesis, the fetus receives

folate and its active metabolites such as tetrahydrofolate (THF) and 5-methyl-tetrahydrofolate (5mTHF)³⁰ exclusively from circulation. As 5mTHF is the main form of folate in blood,³⁰ the level of RFC1, the major transporter that is highly expressed in cardiac tissue to uptake 5mTHF and folate, should be critical for heart development.³¹ Indeed, RFC1 knockout results in embryonic death shortly after implantation.³²⁻³⁴ We have demonstrated that the overexpression of *FIGN* leads to the accumulation of RFC1, and subsequently, to higher intracellular folate levels. The intracellular folate enrichment effect promoted by *FIGN* overexpression was more obvious when the concentration of extracellular folate was close to that in physiological conditions (Figure 6b). These results partly explain the protective effects of the +94762C allele against CHD through increased *FIGN* expression. Given that irrespective of folic acid fortification, up to 16% of circulating and intracellular folate in most individuals is represented by unmetabolized folic acid,³⁵⁻³⁸ the decrease in CHD risk associated with the +94762C allele may be completely explained by the upregulation of folate content as well as its utilization. Remarkably, *FIGN* overexpression also increased the protein expression of DHFR, an enzyme responsible for the reduction of folic acid to 7,8-DHF and subsequently to THF, which is a slow process for folate recycling in humans;³⁹ accordingly, DHFR inhibition by methotrexate leads to the development of CHD in animal models.^{40,41} Collectively, these data indicate that the +94762G>C SNP protects from CHD by stimulating the transmembrane transport and utilization of folate species.

The increase in circulating folate levels is an established approach to prevent CHD, and it is essential to decipher the complex network of folate metabolism and identify the critical players. Our study revealed two facts. First, folate transport and utilization is also regulated by non-folate

metabolic enzymes such as FIGN; therefore, it is important to continue searching for additional factors that can influence folate turnover. Second, circulating folate levels may be defined by multiple regulatory molecules, including those currently unknown, which can be associated with CHD onset irrespectively of their effect on blood folate levels. Thus, the low circulating folate levels in +94762C allele carriers did not correspond to high homocysteine levels. These findings suggest that CHD predictive markers better than circulating folate should be explored. Our initial observations only included the Han Chinese population, but we anticipate that similar findings will be made in other ethnic groups.

In summary, the current study indicates that the *FIGN* +94762G>C polymorphism reduced the risk of CHD by activating the transcription of an alternative *FIGN* isoform, thereby inhibiting proteasome activity and allowing the accumulation of RFC1 and DHFR, which ultimately promoted folate transmembrane transport and utilization. Our findings highlight that enhanced folate utilization through *FIGN* is a promising strategy to prevent CHD via folate fortification.

Sources of Funding

This work is supported by the 973 programs of China (2013CB945400, 2015CB943300, and 2012CB910103), 863 program of China (2015AA020913), National Natural Science Foundations of China (81471454, 31330023, 81430005, and 31521003), International Cooperative grant from Minister of Science and Technology (2014DFA30630) and Science and Technology Municipal Commission of Shanghai (14ZR1402000 and 15XD1500500).

Disclosures

None

References

1. van der Linde D, Konings EE, Slager MA, Witsenburg M, Helbing WA, Takkenberg JJ, Roos-Hesselink JW. Birth prevalence of congenital heart disease worldwide: a systematic review and meta-analysis. *J Am Coll Cardiol.* 2011; 58:2241-2247.
2. Botto LD, Correa A. Decreasing the burden of congenital heart anomalies: an epidemiologic evaluation of risk factors and survival. *Prog Pediatr Cardiol.* 2003; 18:111-121.
3. Czeizel AE, Dudas I, Vereczkey A, and Banhidy F. Folate deficiency and folic acid supplementation: the prevention of neural-tube defects and congenital heart defects. *Nutrients.* 2013; 5:4760-4775.
4. Feng Y, Wang S, Chen R, Tong X, Wu Z, and Mo X. Maternal folic acid supplementation and the risk of congenital heart defects in offspring: a meta-analysis of epidemiological observational studies. *Sci Rep.* 2015; 5:8506.
5. Frosst P, Blom HJ, Milos R, Goyette P, Sheppard CA, Matthews RG, Boers GJH, den Heijer M, Kluijtmans LAJ, van den Heuvel LP, and Rozen R. A candidate genetic risk factor for vascular disease: a common mutation in methylenetetrahydrofolate reductase. *Nat Genet.* 1995; 10:111-113.
6. Weisberg I, Tran P, Christensen B, Sibani S, and Rozen R. A second genetic polymorphism in methylenetetrahydrofolate reductase (*MTHFR*) associated with decreased enzyme activity. *Mol Genet Metab.* 1998; 64:169-172.
7. Brattstrom L, Wilcken DEL, Ohrvik J, and Brudin L. Common methylenetetrahydrofolate reductase gene mutation leads to hyperhomocysteinemia but not to vascular disease. *Circulation.* 1998; 98:2520-2526.
8. Xuan C, Li H, Zhao JX, Wang HW, Wang Y, Ning CP, Liu Z, Zhang BB, He GW, and Lun LM. Association between *MTHFR* polymorphisms and congenital heart disease: a meta-analysis based on 9,329 cases and 15,076 controls. *Sci Rep.* 2014; 4:7311.
9. Christensen KE, Rohicek CV, Andelfinger GU, Michaud J, Bigras JL, Richter A, Mackenzie RE, and Rozen R. The *MTHFD1* p.Arg653Gln variant alters enzyme function and increases risk for congenital heart defects. *Hum Mutat.* 2009; 30:212-220.
10. Zhao JY, Qiao B, Duan WY, Gong XH, Peng QQ, Jiang SS, Lu CQ, Chen YJ, Shen HB, Huang GY, Jin L, Wang HY. Genetic variants reducing *MTR* gene expression increase risk of congenital heart disease in Han Chinese population. *Eur Heart J.* 2014; 35:733-742.
11. Zhao JY, Yang XY, Gong XH, Gu ZY, Duan WY, Wang J, Ye ZZ, Shen HB, Shi KH, Hou J, Huang GY, Jin L, Qiao B, Wang HY. A functional variant in *MTRR* intron-1 significantly increases risk of congenital heart disease in Han Chinese population. *Circulation.* 2012; 125:482-490.

12. Zhao JY, Yang XY, Shi KH, Sun SN, Hou J, Ye ZZ, Wang J, Duan WY, Qiao B, Chen YJ, Shen HB, Huang GY, Jin L, Wang HY. A functional variant in the cystathionine β -synthase gene promoter significantly reduces congenital heart disease susceptibility in a Han Chinese population. *Cell Res.* 2013; 23:242-253.
13. Wang J, Zhao JY, Wang F, Peng QQ, Hou J, Sun SN, Gui YH, Duan WY, Qiao B, and Wang HY. A genetic variant in vitamin B12 metabolic genes that reduces the risk of congenital heart disease in Han Chinese populations. *PLoS One.* 2014; 9:e88332.
14. Botto LD, Mulinare J, Erickson JD. Occurrence of congenital heart defects in relation to maternal multivitamin use. *Am J Epidemiol.* 2000; 151:878-884.
15. Botto LD, Mulinare J, Erickson JD. Do multivitamin or folic acid supplements reduce the risk for congenital heart defects? Evidence and gaps. *Am J Med Genet PART A.* 2003; 121:95-101.
16. Hernandez-Diaz S, Werler MM, Walker AM, and Mitchell AA. Folic acid antagonists during pregnancy and the risk of birth defects. *N Engl J Med.* 2000; 343:1608-1614.
17. Hobbs CA, Cleves MA, Melnyk S, Zhao W, and James SJ. Congenital heart defects and abnormal maternal biomarkers of methionine and homocysteine metabolism. *Am J Clin Nutr.* 2005; 81:147-153.
18. Sutton M, Mills JL, Molloy AM, Troendle JF, Brody LC, Conley M, McDonnell R, Scott JM, and Kirke PN. Maternal vitamin levels in pregnancies affected by congenital malformations other than neural tube defects. *Birth Defects Res A Clin Mol Teratol.* 2011; 91:610-615.
19. Kapusta L, Haagmans ML, Steegers EA, Cuypers MH, Blom HJ and Eskes TK. Congenital heart defects and maternal derangement of homocysteine metabolism. *J Pediatr.* 1999; 135:773-774.
20. Tanaka T, Scheet P, Giusti B, Bandinelli S, Piras MG, Usala G, Lai S, Mulas A, Corsi AM, Vestriini A, Sofi F, Gori AM, Abbate R, Guralnik J, Singleton A, Abecasis GR, Schlessinger D, Uda M, Ferrucci L. Genomewide association study of vitamin B6, vitamin B12, folate, and homocysteine blood concentrations. *Am J Hum Genet.* 2009; 84:477-482.
21. Hazra A, Kraft P, Lazarus R, Chen C, Chanock SJ, Jacques P, Selhub J, Hunter DJ. Genome-wide significant predictors of metabolites in the one-carbon metabolism pathway. *Hum Mol Genet.* 2009; 18:4677-4687.
22. Cox GA, Mahaffey CL, Nystuen A, Letts VA, Frankel WN. The mouse fidgetin gene defines a new role for AAA family proteins in mammalian development. *Nat Genet.* 2000; 26:198-202.
23. Robert J, Tomko J and Mark H. Molecular architecture and assembly of the eukaryotic proteasome. *Annu Rev Biochem.* 2013; 82:415-445.
24. Halwachs S, Schaefer I, Seibel P, Honscha W. Antiepileptic drugs reduce the efficacy of methotrexate chemotherapy through accelerated degradation of the reduced folate carrier by the ubiquitin-proteasome pathway. *Chemotherapy.* 2011; 57:345-356.
25. Amici M, Sagratini D, Pettinari A, Pucciarelli S, Angeletti M, Eleuteri AM. 20S proteasome mediated degradation of DHFR: implications in neurodegenerative disorders. *Arch Biochem Biophys.* 2004; 422:168-174.

26. Safi J, Joyeux L, Chalouhi GE. Periconceptional folate deficiency and implications in neural tube defects. *J Pregnancy*. 2012; 2012:295083.
27. Seo SR, Chung KC. CREB activates proteasomal degradation of SDCR1/RCAN1. *FEBS Letters*. 2008; 582:1889-1893.
28. Hoang T, Fenne IS, Madsen A, Bozickovic O, Johannessen M, Bergsvåg M, Lien EA, Stallcup MR, Sagen JV, Moens U, Mellgren G. cAMP response element binding protein interacts with and stimulates the proteasomal degradation of the nuclear receptor coactivator grip1. *Endocrinology*. 2013; 154:1513-1527.
29. Bruneau BG. The developmental genetics of congenital heart disease. *Nature*. 2008; 451:943-948.
30. Smith AD, Kim YI, Refsum H. Is folic acid good for everyone? *Am J Clin Nutr*. 2008; 87:517-533.
31. Maddox DM, Manlapat A, Roon P, Prasad P, Ganapathy V, Smith SB. Reduced-folate carrier (RFC) is expressed in placenta and yolk sac, as well as in cells of the developing forebrain, hindbrain, neural tube, craniofacial region, eye, limb buds and heart. *BMC Dev Biol*. 2003; 3:6.
32. Gelineau-van WJ, Heller S, Bauer LK, Wilberding J, Maddox JR, Aleman F, Rosenquist TH, Finnel RH. Embryonic development in the reduced folate carrier knockout mouse is modulated by maternal folate supplementation. *Birth Defects Res A Clin Mol Teratol*. 2008; 82: 494-507.
33. Matherly LH, Goldman DI. Membrane transport of folates. *Vitam Horm*. 2003; 66: 403-456.
34. Sirotnak FM, Tolner B. Carrier-mediated membrane transport of folates in mammalian cells. *Annu Rev Nutr*. 1999; 19: 91-122.
35. Troen AM, Mitchell B, Sorensen B, Wener MH, Johnston A, Wood B, Selhub J, McTiernan A, Yasui Y, Oral E, Potter JD, Ulrich CM. Unmetabolized folic acid in plasma is associated with reduced natural killer cell cytotoxicity among postmenopausal women. *J Nutr*. 2006; 136:189-194.
36. Sweeney MR, McPartlin J, Weir DG, Daly S, Pentieva K, Daly L, Scott JM. Evidence of unmetabolised folic acid in cord blood of newborn and serum of 4-day-old infants. *Br J Nutr*. 2005; 94:727-730.
37. Rock CL. Multivitamin-multimineral supplements: who uses them? *Am J Clin Nutr*. 2007; 85:277S-9.
38. Pfeiffer CM, Fazili Z, McCoy L, Zhang M, Gunter EW. Determination of folate vitamers in human serum by stable-isotope-dilution tandem mass spectrometry and comparison with radio assay and microbiologic assay. *Clin Chem*. 2004; 50:423-432.
39. Bailey SW, Ayling JE. The extremely slow and variable activity of dihydrofolate reductase in human liver and its implications for high folic acid intake. *Proc Natl Acad Sci U S A*. 2009; 106:15424-15429.
40. Sun S, Gui Y, Jiang Q, Song H. Dihydrofolate reductase is required for the development of heart and outflow tract in zebrafish. *Acta Biochim Biophys Sin (Shanghai)*. 2011; 43:957-969.

41. Lee MS, Bonner JR, Bernard DJ, Sanchez EL, Sause ET, Prentice RR, Burgess SM, Brody LC. Disruption of the folate pathway in zebrafish causes developmental defects. *BMC Dev Biol.* 2012; 12:12.



Circulation

Table 1. Association between *FIGN* +94762G>C and congenital heart disease in the Han Chinese

Group	Genotype	Control	Case	OR (95% CI) *	<i>P</i> †	HWE <i>P</i> ‡
Shanghai	GG	195 (60.8%)	220 (72.4%)	1.00	0.0048	0.21
	GC	105 (32.7%)	74 (24.3%)	0.52 (0.35-0.78)		
	CC	21 (6.5%)	10 (3.3%)	0.36 (0.15-0.88)		
	G	495 (77.1%)	514 (84.5%)	1.00	0.001	
	C	147 (22.9%)	94 (15.5%)	0.61 (0.46-0.81)		
Shandong	GG	359 (58.9%)	417 (73.9%)	1.00	0.0012	0.10
	GC	208 (34.1%)	134 (23.8%)	0.60 (0.44-0.82)		
	CC	43 (7.0%)	13 (2.3%)	0.23 (0.11-0.49)		
	G	926 (75.9%)	968 (85.8%)	1.00	7.7×10⁻⁵	
	C	294 (24.1%)	160 (14.2%)	0.52 (0.42-0.65)		
Anhui	GG	440 (54.1%)	399 (64.2%)	1.00	0.0041	0.93
	GC	316 (38.8%)	196 (31.6%)	0.65 (0.48-0.90)		
	CC	58 (7.1%)	26 (4.2%)	0.43 (0.22-0.83)		
	G	1,196 (73.5%)	994 (80.0%)	1.00	1.3×10⁻⁴	
	C	432 (26.5%)	248 (20.0%)	0.69 (0.58-0.82)		
Combined	GG	994 (57.0%)	1,036 (69.6%)	1.00	8.5×10⁻¹³	0.11
	GC	629 (36.0%)	404 (27.1%)	0.56 (0.47-0.67)		
	CC	122 (7.0%)	49 (3.3%)	0.34 (0.23-0.50)		
	G	2,617 (75.0%)	2,476 (83.1%)	1.00	5.1×10⁻¹⁴	
	C	873 (25.0%)	502 (16.9%)	0.61 (0.54-0.69)		

* Adjusted for age and sex; †*P*-value for the Chi-square test and corrected by Bonferroni correction;

‡*P*-value for the Hardy–Weinberg equilibrium test in control subjects

Figure Legends

Figure 1. *FIGN* +94762C allele is associated with reduced plasma folate and homocysteine in Han Chinese population. Human plasma folate (a) and homocysteine (b) levels. Data are presented as the means \pm standard error (SE). Actual folate levels for each genotype were: GG = 12.94 ± 0.66 ng/ml, GC = 11.56 ± 0.80 ng/ml, and CC = 8.72 ± 1.96 ng/ml, and homocysteine levels were: GG = 11.33 ± 1.41 μ mol/l, GC = 10.41 ± 2.03 μ mol/l, and CC = 9.96 ± 1.12 μ mol/l. * $P < 0.05$, ** $P < 0.01$, # $P > 0.05$.



Figure 2. *FIGN* +94762C is correlated with the upregulation of *FIGN* expression. (a) In the upper panel, the position of the *FIGN* +94762G>C polymorphism is indicated. An alternative promoter around the +94762 site is located in *FIGN* intron 4 containing conventional *cis*-regulatory elements (marked). The reporter gene assay construct is presented. The lower panel shows alternative *FIGN* isoforms extracted from the NCBI database; green blocks highlight the coding regions. (b) *FIGN* mRNA levels in tissue samples from individuals with different *FIGN* genotypes at the +94762 site; the numbers of samples with each genotype were: GG = 21, GC = 19, CC = 10. (c) Cross-intron primers used for expression analysis of alternative *FIGN* isoforms. X1, X3, and X4 isoform transcripts were detected in human cardiovascular tissues. (d) Expression of each *FIGN* isoform was quantified by absolute qRT-PCR in three human cardiovascular tissue samples. (e) Variations in *FIGN* isoform X3 expression among individuals with different *FIGN* +94762G>C genotypes. The numbers of samples with each

genotype were: GG = 21, GC = 19, CC = 10. (f) The +94762C allele is associated with the upregulation of FIGN, RFC1 and DHFR proteins. Western blotting analysis of 18 cardiovascular tissue samples obtained from CHD patients: left panel, gel images; right panel, quantification of protein expression. All data are presented as the means \pm standard deviation (SD). * $P < 0.05$, ** $P < 0.01$, # $P > 0.05$.

Figure 3. The +94762C allele activates *FIGN* isoform X3 transcription by inhibiting transcriptional repressor binding. (a) Luciferase expression was significantly increased in cells transfected with the minor C allele construct compared to those transfected with the major G allele construct. The overexpression of exogenous CREB1 downregulated the luciferase activity in both cell groups and reduced the difference between the C allele- and G allele-transfected cells. The expression of exogenous CREB1 was showed in the lower panel. (b) Binding affinity of the purified CREB1 protein to DNA probes containing the +94762G or C alleles. The SPR binding affinity of the G allele ($-\log_{10}K_d = 9.42 \pm 0.61$) was 1,000-fold higher compared to that of the C allele ($-\log_{10}K_d = 6.30 \pm 0.52$). (c) Binding of CREB1 and RNA polymerase II (Pol II) to *FIGN* intron 4 in HEK293T cells analyzed using chromatin immunoprecipitation (ChIP) assays. (d) ChIP assay in human cardiovascular tissues. The CC genotype attenuates CREB1 binding affinity to *FIGN* intron 4 and increases the binding of Pol II. (e) CREB1 knockdown increases the expression of *FIGN* mRNA (left panel) and protein (right panel) in HEK293T cells. All data are presented as the means \pm SD of three independent experiments. * $P < 0.05$, ** $P < 0.01$.

Figure 4. FIGN inhibits proteasome activity through direct interaction with proteasome

subunits. (a) Gene ontology enrichment analysis showed that FIGN-interacting proteins identified by proteomics using tandem affinity purification were enriched for proteasome-related functions. (b–d) Co-immunoprecipitation assays validated that FIGN interacted with PSMD4 (b), PSMC5 (c), and PSMD13 (d). (e) Expression of PSMD4, PSMD13, and PSMC5 in cultured cells overexpressing FIGN. (f) The upper panel shows increased FIGN expression inhibited proteasome activity in different cells. The lower panel shows FIGN expression levels in cells transfected with Flag-tagged FIGN. The data are presented as the means \pm SD of three independent experiments. * $P < 0.05$.



Figure 5. FIGN blocks the degradation of RFC1 and DHFR. (a–c) RFC1 and DHFR expression in the wild-type (a), FIGN-overexpressing (b), or FIGN-knocking down (c) HEK293T cells treated with either cycloheximide (CHX) or DMSO (Control), for various times. (d) RFC1 and DHFR levels in cells treated with proteasome inhibitor MG132. (e) FIGN overexpression in HEK293T cells and HDFs resulted in the accumulation of RFC1 and DHFR at the protein level but not the mRNA level. (f) FIGN overexpression-induced increase in RFC1 and DHFR levels was saturated by MG132. (g) CREB1 knockdown activated FIGN expression and increased protein levels of RFC1 and DHFR.

Figure 6. Increased FIGN expression promotes folate transmembrane transport and

metabolism. (a) In HEK293T cells cultured in high folate medium (1 $\mu\text{g/ml}$), the increase in FIGN expression upregulated intracellular folate levels by 72%. (b) In HEK293T cells cultured in low folate medium (10 ng/ml), increased FIGN expression upregulated intracellular folate level by 50% and reduced extracellular folate level by 35%. (c) Extracellular folate levels were decreased in the FIGN-overexpressing HDFs and H9C2 cells. (d) Increased FIGN expression caused 24% and 32% decreases of homocysteine in cells maintained in high-and low-folate conditions, respectively. (e) Increased FIGN expression elevated SAM concentration by 37% and the ratio of SAM to SAH by 49%. (f) EDU staining showed that increased FIGN expression upregulated DNA synthesis by 110%. (g) Growth of the wild-type and FIGN-overexpressing HEK293T cells under high-and low-folate conditions. (h) *Fign* mRNA transcription in embryonic (E12, E16, E20), neonatal (Neo), and adult cardiac tissues of mice. (i) *Fign* mRNA (lower panel) and FIGN protein (upper panel) expression in maternal and corresponding fetal rat hearts analyzed by qRT-PCR and western blotting, respectively. (j) *FIGN* mRNA (lower panel) and protein (upper panel) expression in the human chorion and corresponding decidua analyzed by qRT-PCR and western blotting, respectively. All data are presented as the means \pm SD of three independent experiments. * $P < 0.05$, ** $P < 0.01$.

Figure 7. The +94762C allele decreases plasma folate and increases tissue folate

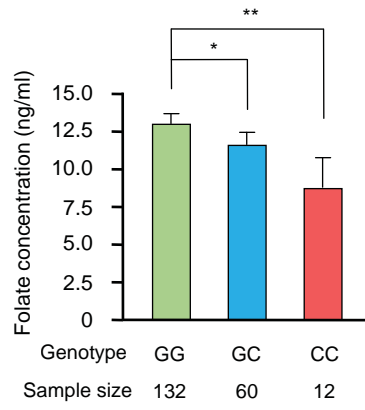
concentrations. (a) Folate concentration in human cardiovascular tissues with different *FIGN* genotypes at the +94762 site. The numbers of samples with each genotype were: GG = 18, GC =

22, CC = 10. (b, c) Folate concentrations in plasma (b) and matched decidua tissues (c) of individuals with different *FIGN* genotypes at the +94762 site (n = 10 per group). (d) Expression of *FIGN* total and isoform X3 mRNA in decidua tissue samples of individuals with different *FIGN* genotypes at the +94762 site (n = 10 per group). (e) The presence of the +94762C allele increases protein expression of FIGN, RFC1, and DHFR. Western blotting analysis of 18 decidua samples is shown: left panel, gel images; right panel, quantification of protein expression. * $P < 0.05$, ** $P < 0.01$, # $P > 0.05$.

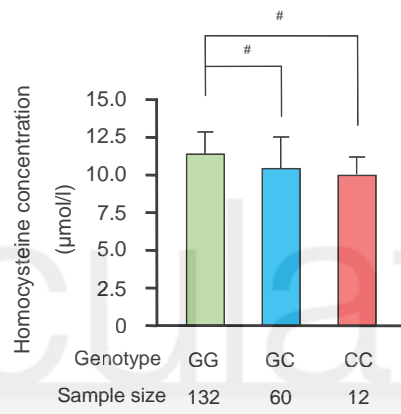


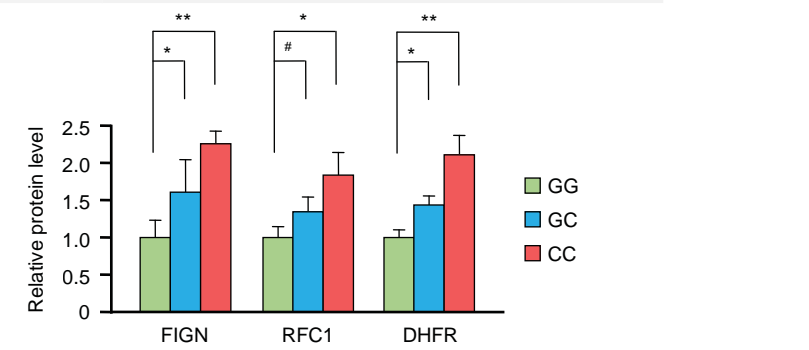
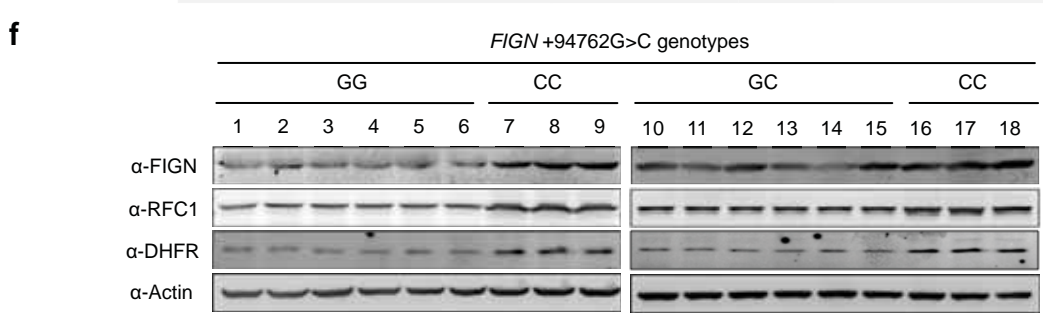
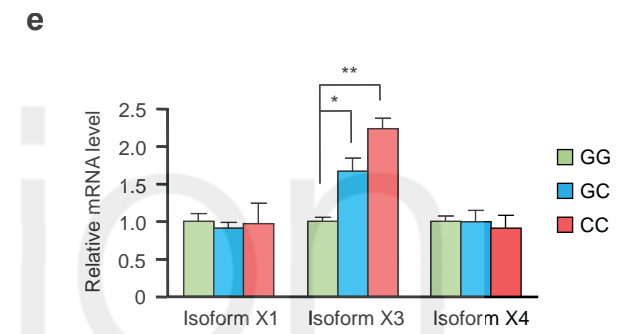
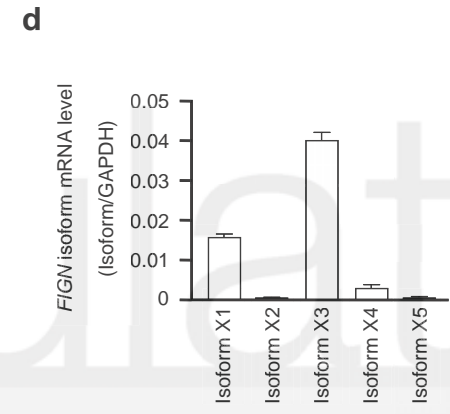
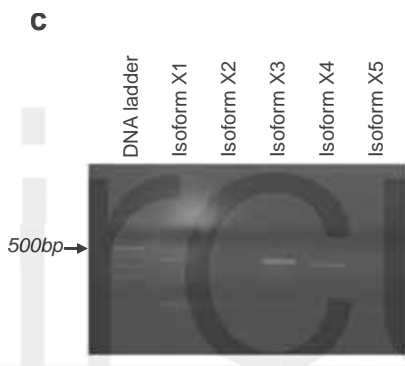
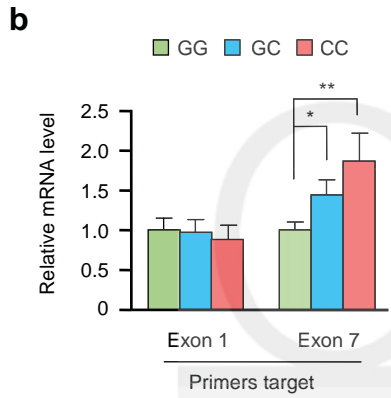
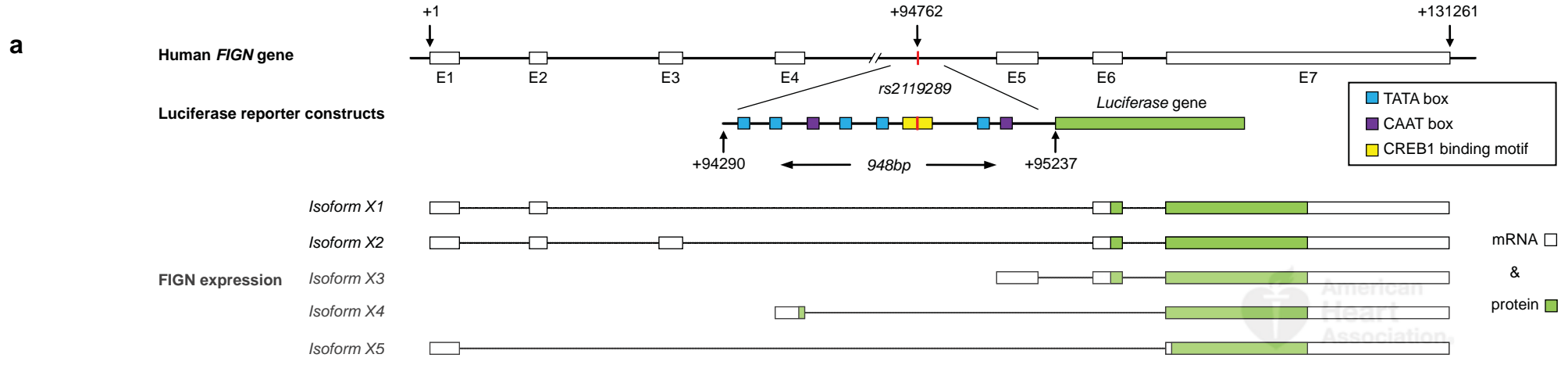
Circulation

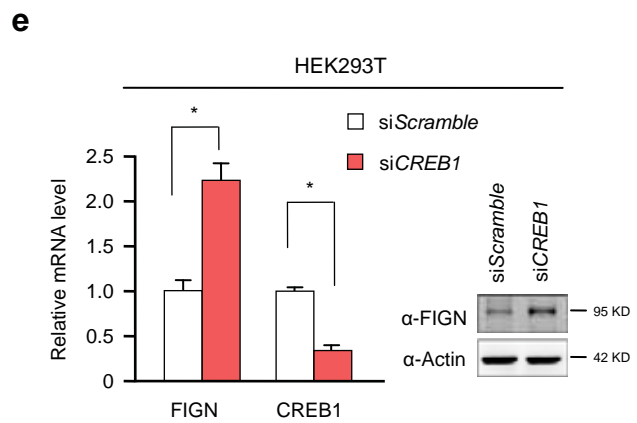
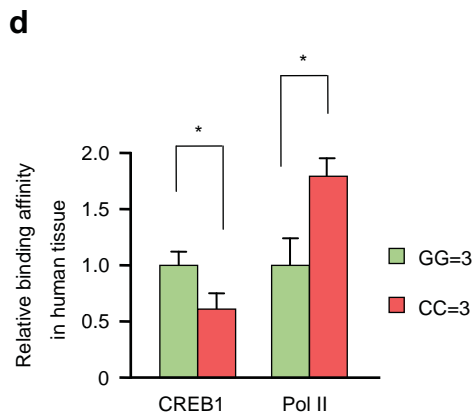
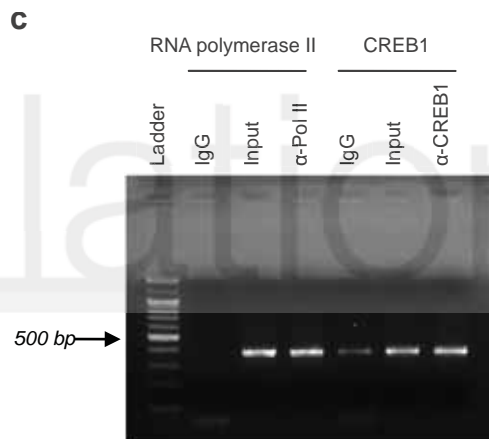
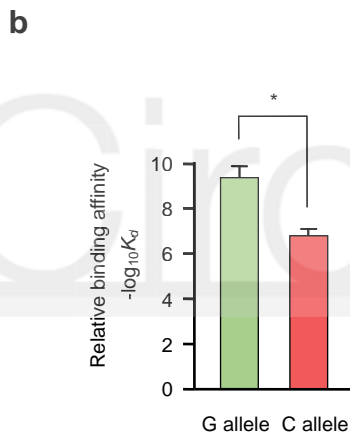
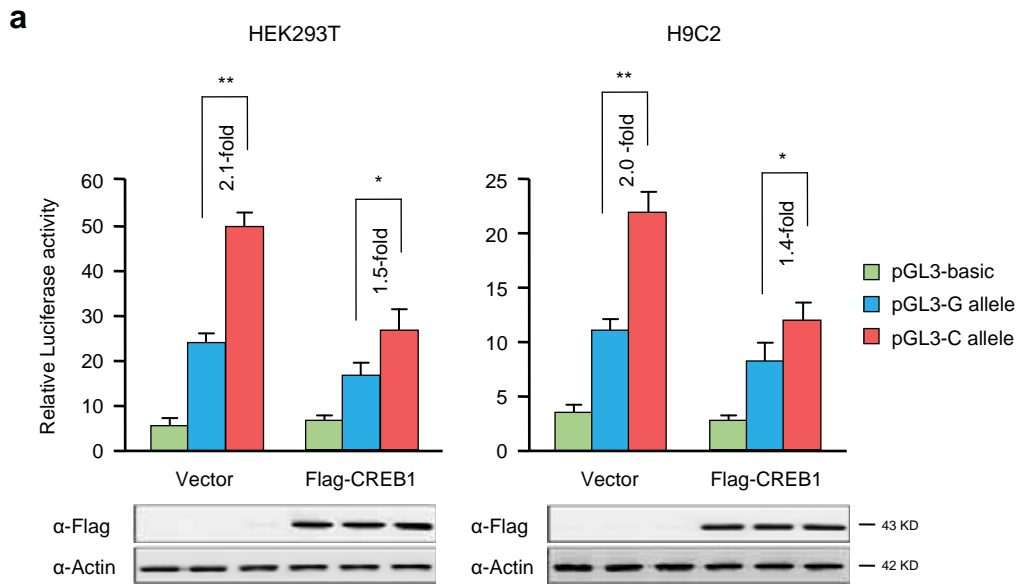
a

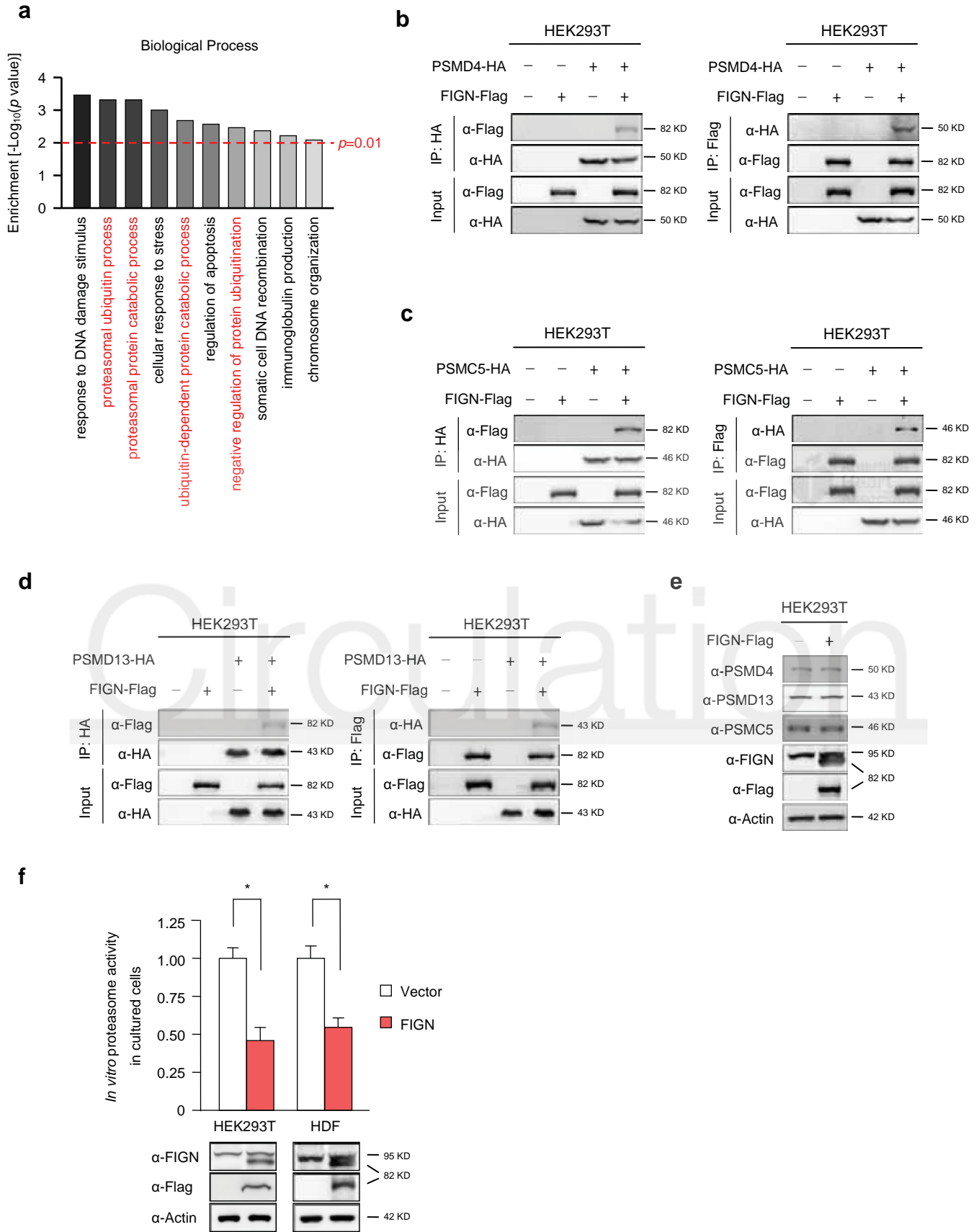


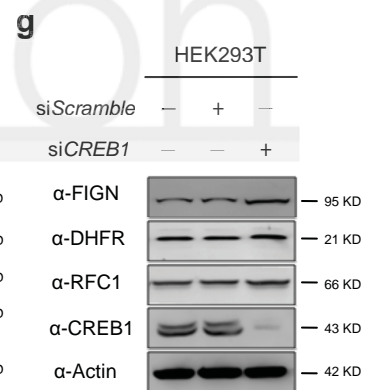
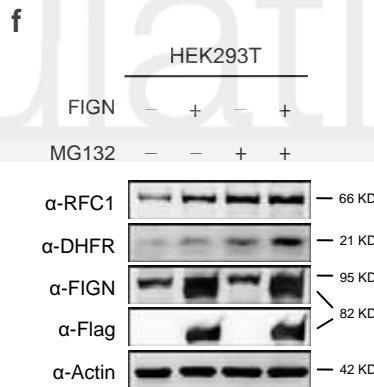
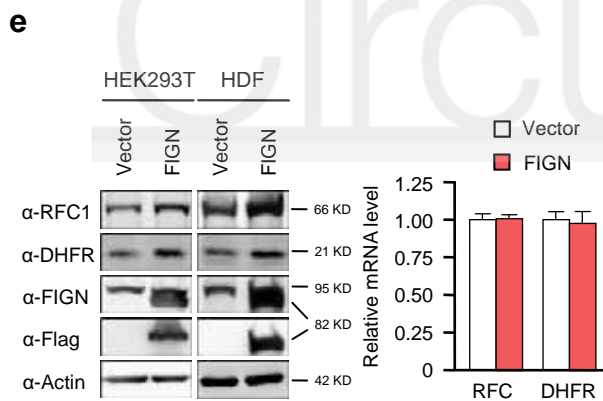
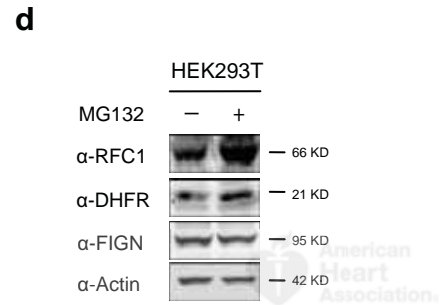
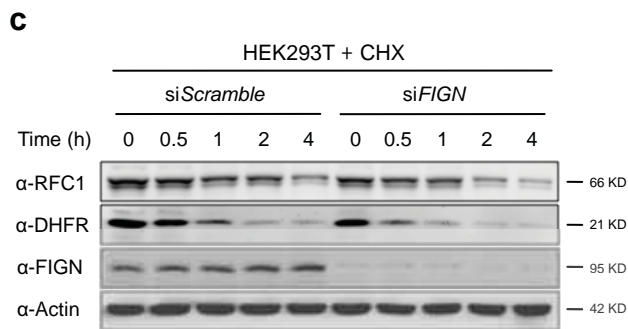
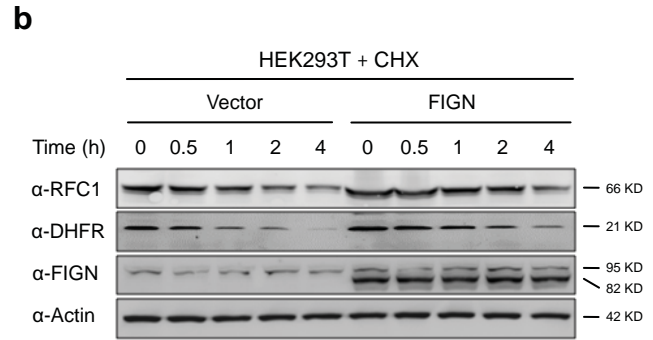
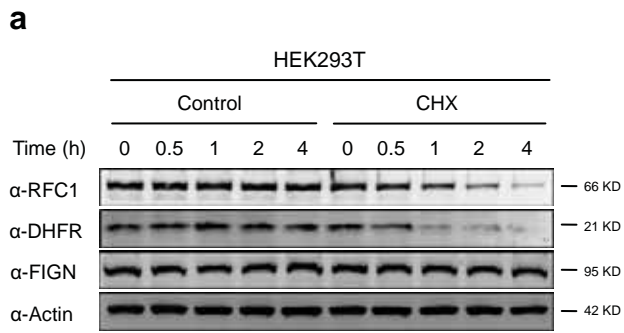
b

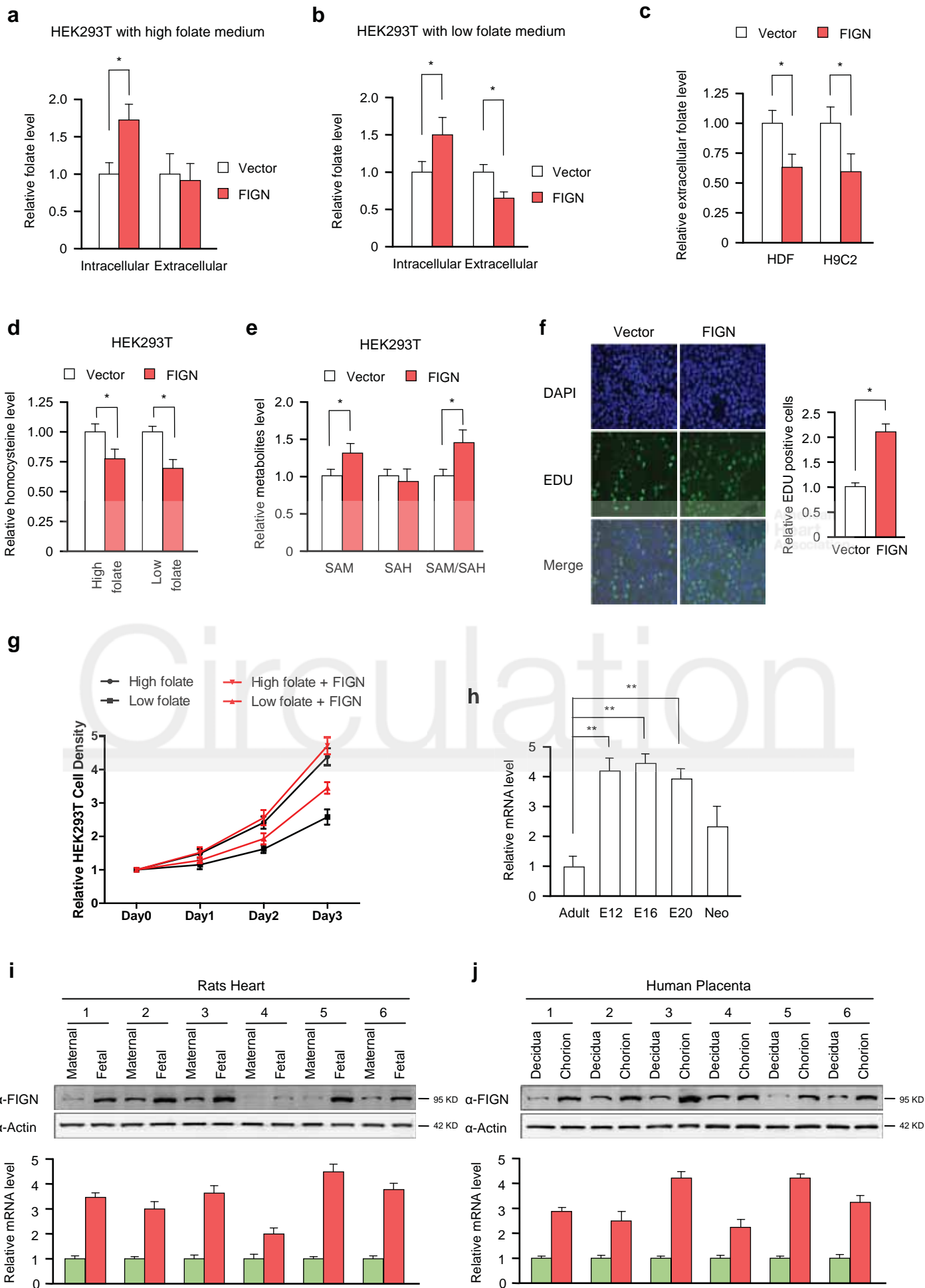


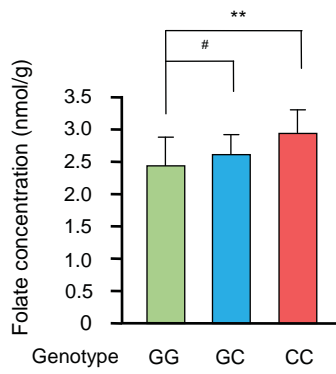
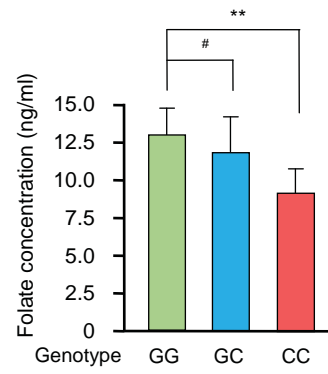
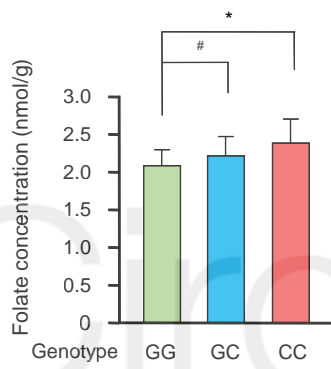
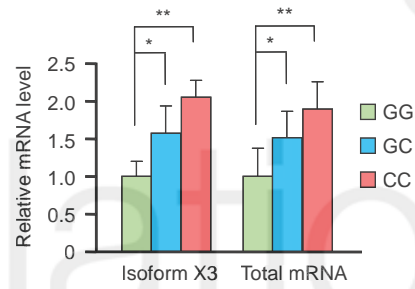
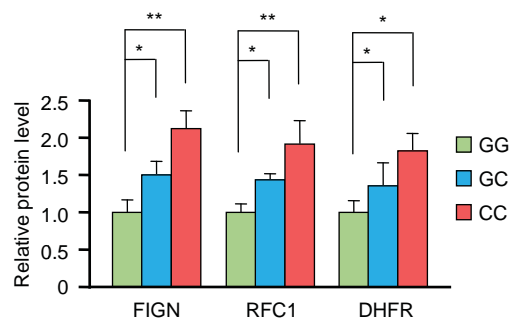
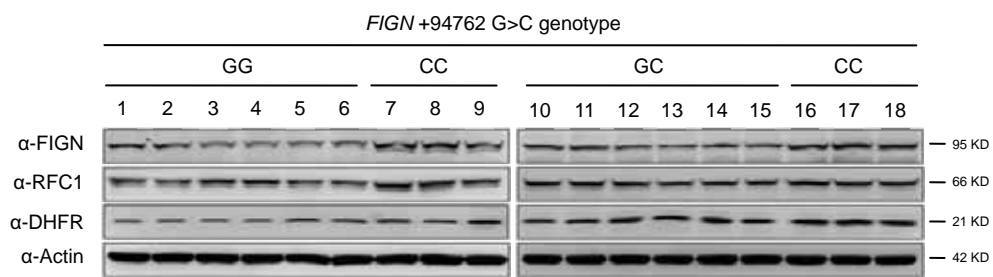










a**b****c****d****e**

Lower Circulating Folate Induced by a Fidgetin Intronic Variant is Associated with Reduced Congenital Heart Disease Susceptibility

Dan Wang, Feng Wang, Kai-Hu Shi, Hui Tao, Yang Li, Rui Zhao, Han Lu, Wenyan Duan, Bin Qiao, Shi-Min Zhao, Hongyan Wang and Jian-Yuan Zhao

Circulation. published online March 16, 2017;

Circulation is published by the American Heart Association, 7272 Greenville Avenue, Dallas, TX 75231

Copyright © 2017 American Heart Association, Inc. All rights reserved.

Print ISSN: 0009-7322. Online ISSN: 1524-4539

The online version of this article, along with updated information and services, is located on the World Wide Web at:

<http://circ.ahajournals.org/content/early/2017/03/15/CIRCULATIONAHA.116.025164>

Data Supplement (unedited) at:

<http://circ.ahajournals.org/content/suppl/2017/03/15/CIRCULATIONAHA.116.025164.DC1>

Permissions: Requests for permissions to reproduce figures, tables, or portions of articles originally published in *Circulation* can be obtained via RightsLink, a service of the Copyright Clearance Center, not the Editorial Office. Once the online version of the published article for which permission is being requested is located, click Request Permissions in the middle column of the Web page under Services. Further information about this process is available in the [Permissions and Rights Question and Answer](#) document.

Reprints: Information about reprints can be found online at:
<http://www.lww.com/reprints>

Subscriptions: Information about subscribing to *Circulation* is online at:
<http://circ.ahajournals.org/subscriptions/>

SUPPLEMENTAL MATERIAL

**Lower Circulating Folate Induced by a Fidgetin Intronic Variant Is
Associated with Reduced Congenital Heart Disease Susceptibility**

SUPPLEMENTAL METHODS

Study Subjects

We analyzed samples from 1,489 CHD patients and 1,745 healthy individuals of three independent case-control groups (Supplemental Table 1). Participants were recruited from Children's Hospital of Fudan University (Shanghai, China) between August 2008 and February 2011, from Cardiovascular Disease Institute, General Hospital of Jinan Military Command (Jinan, Shandong Province, China) between August 2008 and January 2011, and from Second Hospital of Anhui Medical University (Hefei, Anhui Province, China) between August 2009 and February 2016. In the principle component analysis we validated that no significant difference in ancestry-informative biomarkers among the tested cases and controls, avoiding potential artifacts due to population stratification effects.¹ Among the 1,489 CHD patients, 932 had ventricular septal defect (VSD), 193 had atrial septal defect (ASD), 210 had Tetralogy of Fallot, 97 had atrioventricular septal defect, 31 had transposition of the great arteries, and 26 had the double outlet right (or left) ventricle. CHD patients who had clinical features of developmental syndromes, multiple major developmental anomalies, or known chromosomal abnormalities as well as family history of CHD in a first-degree relative (parent, sibling, or child) were excluded. Controls were non-CHD outpatients from the same geographical areas who were matched to CHD patients in sex and age in the same duration (Supplemental Table 1). The exclusion criteria for control subjects were cardiac disease or congenital anomalies in an individual or his/her first-degree relative. All participants were genetically unrelated ethnic Han Chinese.

We obtained 50 human cardiovascular tissue samples, including 11 ventricle, 9 atrium, 14 outlet, 11 aorta, and 5 ventricular septum samples, for quantitative reverse-transcriptase polymerase chain reaction and western blotting; and 50 human cardiovascular tissue samples, including 23 outlet, 14 ventricle and 13 aorta samples, for folate concentration detection, from CHD patients who had undergone heart catheterization or surgery between January 2014 and December 2016 at Children's Hospital of Fudan University.

To explore the association between *FIGN* variants and human plasma folate and homocysteine levels in the Han Chinese population, blood samples of 204 healthy fasting child volunteers were collected during regular physical examination between August 2014 and December 2015 in Children's Hospital of Fudan University.

To determine whether *FIGN* facilitates folate absorption in maternal tissues, 10 pairs of decidua samples and matched blood samples for each *FIGN* genotypes from women who had spontaneous abortion were required from the biobank in Obstetrics & Gynecology Hospital of Fudan University.

SNP Selection and Genotyping

Genomic DNA was isolated from venous blood using conventional protocols. Specific regions of the *SYT9*, *PRICKLE2-AS1*, *GABBR2*, *CACNA1E*, *FIGN*, and *NBPF3* genes were amplified from genomic DNA by PCR. Polymorphisms in *SYT9* (rs11041321), *PRICKLE2-AS1* (rs153734), *GABBR2* (rs10986018), *CACNA1E* (rs1999594), *FIGN* (rs2119289), and *NBPF3* (rs4654748) significantly associated with folate

concentration in GWAS cohorts were identified by genotyping using the SnaPshot kit (ABI, Foster City, CA, USA). The samples for genotyping were run on an ABI 3730 automated sequencer and analyzed using the Peakscan software. For each polymorphism, 30 samples were randomly selected to confirm with DNA sequencing, and the concordant rate was 100%. Sequences of primer pairs are listed in Supplemental Table 4.

Reverse Transcription, PCR and Absolute and Relative qRT-PCR

Total RNA was extracted from human cardiovascular tissue samples preserved in RNAlater (Qiagen, Valencia, CA, USA) and converted to cDNA using specific primers and Moloney murine leukemia virus reverse transcriptase (Takara, Berkeley, CA, USA). *FIGN* total mRNA was measured using primers targeting exon 1 or exon 7. To distinguish between the expression statuses of different *FIGN* isoforms, specific cross exon primers were designed. For isoform X1, the forward primer was located in exon 1 and reverse primer crossed exons 2 and 6; the amplified product had 364 base pairs (bp). For isoform X2, the forward primer crossed exons 2 and 3, and the reverse primer crossed exons 6 and 7; the amplified product had 362 bp. For isoform X3, the forward primer targeted exon 5 and the reverse primer crossed exons 6 and 7; the amplified product had 345 bp. For isoform X4, the forward primer targeted exon 4 and the reverse primer crossed exons 4 and 7; the amplified product had 315 bp. For isoform X5, the forward primer crossed exons 1 and 7 and the reverse primer was located in exon 7; the amplified product had 340 bp.

The relative qRT-PCR was performed in an ABI Prism 7900 sequence detection system in a volume of 10 μ l containing 250 nM of forward and reverse primers, 5 μ l of SYBR Green Supermix (Bio-Rad Laboratories, Hercules, CA, USA), and 10 ng of cDNA. Each sample was run in triplicate, and *GAPDH* was used as an internal reference gene; relative mRNA expression levels were calculated using the Δ Ct method ($2^{-\Delta\Delta C_t}$). The primers are listed in Supplemental Table 4.

In the absolute qRT-PCR, the PCR fragments described above from five *FIGN* isoforms and *GAPDH* were synthesized and cloned in the pMD-19T vector (Invitrogen, Carlsbad, CA, USA). Single colonies of transformed bacteria were inoculated into 25 ml of LB and grown overnight at 37°C with agitation (200 rpm). Purified plasmid DNA was dissolved in 150 μ l TE buffer, and a standard curve was obtained by analyzing six 10-fold serial dilutions of the plasmid using qRT-PCR. Finally, the expression of *FIGN* isoforms in tissue samples was determined by qRT-PCR and calculated as the ratio of *FIGN* isoform copies to *GAPDH* copies.

Plasmid Constructs, Cell Culture, and Transfection

To construct a luciferase reporter plasmid containing *FIGN* variants, a 948-bp fragment from +94,290 to +95,237 bp of *FIGN* intron 4 containing the +94762G allele was amplified from genomic DNA using PCR and cloned into the *Mlu*I and *Hind*III restriction sites of the pGL3-basic vector containing the firefly luciferase gene as a reporter (Promega, Madison, WI, USA). Then, the C allele in the plasmid was generated by site-directed mutagenesis using the MutanBEST kit (Takara, Berkeley,

CA, USA) to ensure uniform backbone sequence (primers are presented in Supplemental Table 4). The whole-length cDNA clones of *FIGN* and cAMP responsive element binding protein 1 (*CREB1*) were purchased from ORIGENE (Rockville, MD, USA).

In the luciferase assay, human embryonic kidney 293T (HEK293T) cells and rat cardiac myocytes (H9C2) were seeded at the density of 1×10^5 cells/well in 24-well culture plates. After 24 h, cells were co-transfected with 1 μ g of the *FIGN* reporter plasmid and 20 ng of the pRL-TK plasmid (Promega) as a normalizing control, while half of the cells were additionally co-transfected with 500 ng the pcDNA3.1-*CREB1* expression plasmid or equivalent amounts of the empty pcDNA3.1 vector using Lipofectamine 2000 (Invitrogen), according to the manufacturer's instructions. After additional 24 h, transfected cells were assayed for luciferase activity using the Dual-Luciferase Reporter Assay System (Promega). Three independent transfection experiments were performed, and each luciferase assay was carried out in triplicate.

To reveal *FIGN* protein function, HEK293T cells or human dermal fibroblasts (HDFs) were transfected with Flag-tagged *FIGN* using Lipofectamine 2000. To knockdown *FIGN* or *CREB1*, HEK293T cells were transfected with specific siRNAs using Lipofectamine RNAiMAX; scramble siRNA was used as control (siRNA sequences are listed in Supplemental Table 4).

Surface Plasmon Resonance (SPR) Analysis

SPR analysis was performed using the ProteOn XPR36 Protein Interaction Array

System (Bio-Rad, Hercules, CA, USA). Biotinylated duplex oligonucleotide probes representing the +94762G or C alleles with 10-bp flanking sequences were each diluted to 400 nM and immobilized on streptavidin-modified surfaces of different channels. The CREB1 protein was purified from *CREB1*-overexpressing HEK293T cells, diluted in PBST to different concentrations, and pre-incubated with non-specific DNA for 15 min before application to the surfaces containing immobilized +94762G or C allele DNA. The results presented in the sensorgram were converted using the BIA evaluation software. Three independent experiments were performed.

Chromatin Immunoprecipitation (ChIP) Assays

ChIP assays were conducted using the EZ ChIP kit (Upstate, Lake Placid, NY, USA). First, HEK293T cells and six cardiac tissue samples (three had the +94762GG and three had the CC genotype) were crosslinked by 1% formaldehyde for 10 min. DNA was then sonicated into fragments with a mean length of 200 to 1,000 bp, and sheared chromatin was immunoprecipitated with antibodies against CREB1, RNA polymerase II (Pol II), or non-specific rabbit IgG (Santa Cruz, Santa Cruz, CA, USA) overnight at 4°C. The precipitated DNA fragments were then identified by PCR and quantified by qRT-PCR (primers are listed in Supplemental Table 4).

Western Blotting

Cells or tissues were homogenized in ice-cold NP40 lysis buffer, and total protein extracts were subjected to western blotting analysis using antibodies specific to FIGN,

RFC1, DHFR, and CREB1 (all from Abcam, Cambridge, MA, USA), and Flag-tag (Abmart, Shanghai, China) according to standard protocols. The predicted band size of FIGN in western blotting was 82 kDa. The observed band size of endogenous and exogenous FIGN were 95 kDa and 82 kDa, respectively. We found the endogenous FIGN had larger observed molecular weight than predicted because of protein glycosylation (Supplemental Figure 3).

Proteasome Activity Measurement

Cellular proteasomal activity was measured using the Proteasome Activity Assay kit (Abcam). Briefly, HEK293T cells and HDFs transfected with *FIGN*-containing plasmid or empty vector were seeded in 96-well plates. After 48 h, cells were harvested, lysed in 0.5% NP40, and centrifuged to collect supernatant, which was incubated with 1 μ l of proteasome substrates at 37°C in the dark. Then, fluorescence was measured at 350/440 nm using a microtiter plate reader (BioTek, VT, USA).

Metabolite Quantification in Human Plasma, Tissues, and Cultured Cells

EDTA-treated plasma samples were obtained from fasting children in the early morning, centrifuged immediately, and stored in a -80°C freezer until analysis for folate and homocysteine content. HEK293 cells and HDFs were transfected with the *FIGN* construct for 24 h and then lysed by sonication. Human cardiac and decidua tissues were homogenized in PBS and supernatants were collected after centrifugation. Then, all samples were analyzed for folate, homocysteine, and

S-adenosylmethionine (SAM) and S-adenosylhomocysteine (SAH). Each test was performed in triplicate and mean values were used for further analysis.

5-Ethynyl-2'-deoxyuridine Staining and Cell Proliferation Assays

For the 5-ethynyl-2'-deoxyuridine (EDU) staining assay, cells were cultured with 20 μ M EDU for 1 h, harvested, washed twice with PBS, and fixed in 4% paraformaldehyde at room temperature. Then, cells were incubated with 0.5 %Triton X-100 in PBS for 20 min at room temperature, and solution containing 215 μ l PBS, 10 μ l of 100mM CuSO₄, 0.6 μ l of 2mM azide, and 25 μ l of 1M sodium ascorbate was added for 30 min at room temperature in the dark. Cells were counterstained with DAPI to visualize nuclei and analyzed by flow cytometry or fluorescence microscopy.

Cell proliferation was measured using the Cell Counting Kit-8 (CCK-8) (Dojindo Laboratories, Kumamoto, Japan). Briefly, transfected HEK293T cells were seeded in 96-well plates and allowed to adhere; then, CCK-8 solution (10 μ l) was added to each well and cells were incubated in a humidified CO₂ incubator at 37°C for 2 h. Cell proliferation was assessed by the absorbance at 450 nm, and expressed as the ratio between treated and untreated cells.

Supplemental Table 1. Demographic characteristics in CHD cases and controls

Variable	Cases		Controls		P value ^a
	No.	%	No.	%	
Stage 1, Shanghai Group	N = 304		N = 321		
Age, years (mean ± SE)	5.08 ± 0.31		4.91 ± 0.22		0.66
Gender					0.37
Male	185	60.9	184	57.3	
Female	119	39.1	137	42.7	
Stage 2, Shandong Group	N = 564		N = 610		
Age, years (mean ± SE)	6.38 ± 0.26		6.81 ± 0.14		0.15
Gender					0.93
Male	287	50.9	312	51.1	
Female	277	49.1	298	48.9	
Stage 3, Anhui Group	N = 621		N = 814		
Age, years (mean ± SE)	4.29 ± 0.16		4.32 ± 0.12		0.87
Gender					0.96
Male	347	55.9	456	56.0	
Female	274	44.1	358	44.0	
Combined samples	N = 1,489		N = 1,745		
Age, years (mean ± SE)	5.24 ± 0.14		5.30 ± 0.09		0.72
Gender					0.80
Male	819	55.0	952	54.6	
Female	670	45.0	793	45.4	
CHD classification					
Septation defects	1,222	82.1			
Conotruncal defects	267	17.9			
Detailed phenotype					
Atrial septal defect	193	12.7			
Ventricular septal defect	932	62.6			
Tetralogy of Fallot	210	14.1			
Others	154	10.6			

^a The comparison of age was performed by Student's *t*-test, and the comparison of gender was performed by 2-tailed χ^2 test. Data shown in the row of age is means ± SE.

Supplemental Table 2. Demographic characteristics in the parents of CHD cases and controls

Variable	Cases		Controls		P value^a
Stage 1, Shanghai Group	Yes	No	Yes	No	
Maternal folic acid intake	299	5	315	6	0.831
Maternal smoke	10	294	9	312	0.724
Maternal drink	7	297	7	314	0.918
Paternal smoke	21	283	19	302	0.614
Paternal drink	14	290	12	309	0.588
Stage 2, Shandong Group	Yes	No	Yes	No	
Maternal folic acid intake	546	18	589	21	0.810
Maternal smoke	31	533	34	576	0.954
Maternal drink	16	548	19	591	0.780
Paternal smoke	85	479	74	536	0.142
Paternal drink	47	517	49	561	0.851
Stage 3, Anhui Group	Yes	No	Yes	No	
Maternal folic acid intake	604	17	796	18	0.522
Maternal smoke	27	594	34	780	0.874
Maternal drink	12	609	11	803	0.385
Paternal smoke	77	544	103	711	0.886
Paternal drink	70	551	67	747	0.052
Combined samples	Yes	No	Yes	No	
Maternal folic acid intake	1,449	40	1,700	45	0.849
Maternal smoke	68	1,421	77	1,668	0.833
Maternal drink	35	1,454	37	1,708	0.658
Paternal smoke	183	1,306	196	1,549	0.351
Paternal drink	131	1,358	128	1,617	0.127

^aThe comparison of demographic characteristics was performed by 2-tailed χ^2 test.

Supplemental Table 3. The SNPs investigated in the association study

SNP ID	Gene	Base change	Location	Group	MAF			Genotype P^b	HWE P^c
					Control	Case	Database ^a		
rs11041321	<i>SYT9</i>	C>T	Intron	Shanghai	0.12	0.12	0.13	0.99	0.6
				Shandong	0.12	0.13		0.95	0.46
rs153734	<i>PRICKLE2-AS1</i>	T>C	Intron	Shanghai	0.24	0.24	0.32	0.58	0.54
				Shandong	0.39	0.37		0.52	0.61
rs10986018	<i>GABBR2</i>	T>C	Intron	Shanghai	0.01	0.01	0.05	0.46	1.00
				Shandong	0.00	0.00		0.08	1.00
rs199959	<i>CACNA1E</i>	C>T	Intron	Shanghai	0.38	0.34	0.35	0.07	0.08
				Shandong	0.36	0.34		0.22	0.22
rs2119289	<i>FIGN</i>	G>C	Intron	Shanghai	0.23	0.15	0.17	0.0048	0.21
				Shandong	0.24	0.14		0.0012	0.10
rs4654748	<i>NBPF3</i>	T>C	Intron	Shanghai	0.39	0.41	0.38	0.76	0.48
				Shandong	0.37	0.37		0.78	0.55

^aMAF, minor allele frequency from the HapMap database for the CHB population. The difference in the genotype distributions between the case and control subjects was estimated by ^b P value for the chi-square test and corrected by Bonferroni correction. ^c P value for the Hardy-Weinberg equilibrium test in the control subjects.

Supplemental Table 4. DNA sequence of all used primers and siRNA

PRIMER NAME	SEQUENCE (5'-3')	PURPOSE	PRIMER NAME	SEQUENCE (5'-3')	PURPOSE
Sequencing & Genotyping			qRT-PCR		
rs11041321-F	ACA TAG GTG GGA CCC TGA CTC	PCR	FIGN-RT	TAT CAC TGA CTG CAA CCA AAC A	Reverse-transcription
rs11041321-R	TGT TCC AGG TTT GTA GAA GAT TTG	PCR	Isoform1-F	CTC TCC TTT GAA AAC TGA TC	PCR/Real-time PCR
rs11041321-typing	GGT GAG AGT TGG CTT GCT GC	SNaPshot	Isoform1-R	TGT TGA GTC TCA TAA ACA CT	PCR/Real-time PCR
rs153734-F	GGC GGG TCT TGC TAT GTT G	PCR	Isoform2-F	ACC AGT GTT TAT GAG TAG CCT	PCR/Real-time PCR
rs153734-R	TTA GGG ACT TGC TGG ATG CT	PCR	Isoform2-R	CAC TGC ATC TTC AAG CCT CTC	PCR/Real-time PCR
rs153734-typing	CAC TCC CAA GTC CTT GTG ATT AG	SNaPshot	Isoform3-F	TGT AGA TTT TAT GCC ATA TTT TA	PCR/Real-time PCR
rs10986018-F	CTG CCT GAC TCA CCC TGC TC	PCR	Isoform3-R	CAC TGC ATC TTC AAG CCT CTC	PCR/Real-time PCR
rs10986018-R	AAC CCT GCC TTT CAA CAC C	PCR	Isoform4-F	CTC TTC TCC TTG GGA AAT GCA TA	PCR/Real-time PCR
rs10986018-typing	CTC AGT CTG CCC ATT ATT CTA CTT T	SNaPshot	Isoform4-R	ACT GCA TCT TCA AGC CTT GAG	PCR/Real-time PCR
rs199959-F	TGC CCT GGT CCA TGT TCT G	PCR	Isoform5-F	CTC TCC GCG CGT TCA GGC TTG A	PCR/Real-time PCR
rs199959-R	AAG GGA TAG GAG GGA GGA AAG	PCR	Isoform5-R	CTT CTG AAT TCA AGG AAG GC	PCR/Real-time PCR
rs199959-typing	GGC TCT GTG CCG GTC TGA G	SNaPshot	FIGN-F1	ACA TGG CAG AGG CTG CAG T	Real-time PCR
rs2119289-F	CTT GCT GTG GAT TTC CCT CA	PCR	FIGN-R1	CTC ACA AGC ACT GAA CGC GC	Real-time PCR
rs2119289-R	CAT CGG ATT TCT AAC TCA TTT GC	PCR	FIGN-F2	CCA AAT AAG AGA GGC TTG AA	Real-time PCR
rs2119289-typing	CAC ATA GCT TGA AAG GAA TTT GTA	SNaPshot	FIGN-R2	CAA AAT GCC GGA ATA CTT C	Real-time PCR
rs4654748-F	GGT GTC TGT CCA TCT ATC CCT G	PCR	DHFR-F	ATG CCT TAA AAC TTA CTG AAC AAC CA	Real-time PCR
rs4654748-R	TGT TAT GAA ATG GCC TCC CA	PCR	DHFR-R	TGG GTG ATT CAT GGC TTC CT	Real-time PCR
rs4654748-typing	ATA GGG GTG TGG GGT AAT GTC	SNaPshot	RFC1-F	AGT TCC TCG TGC CCA T	Real-time PCR
Plasmid construction			RFC1-R	GTC CGA GAC AAT GAA AGT GAT	Real-time PCR
FIGN-Luc-F	CGA CGC GTC GTA GAT TCT ATA AAT GCA AGA CTT CA	PCR	GAPDH-F	GAA GGT GAA GGT CGG AGT C	Real-time PCR
FIGN-Luc-R	CCC AAG CTT GGG CTG GAA ACC CAC AGC TAG CCA	PCR	GAPDH-R	GAA GAT GGT GAT GGG ATT TC	Real-time PCR
Chromatin immunoprecipitation			M-Isoform1-F	TTG TGA GAA ATC CAA TTC AGC TTT	PCR/Real-time PCR
FIGN-intron4-F	ACT CAT TTG CCT CTG AAG GAG	ChIP-PCR	M-Isoform2-F	AGG TCT TTA TGT ATG GAC ACA AAG	PCR/Real-time PCR
FIGN-intron4-R	GAA AAG AGA GTG TCC AGA GTA	ChIP-PCR	M-Isoform1/2-R	GTG ATG TCA AAG TGC TGT TCT	PCR/Real-time PCR
siRNA			M-Isoform3-F	ACT CCA CCT CTT GCA TAG AGC TCT	PCR/Real-time PCR
siFIGN	GCG ATG CAT CTG CCC AAT GT	Knocking-down	M-Isoform3-R	TCC TCC CAA GAC CTA GAA TTC TAT	PCR/Real-time PCR
siCREB1	GAG AGA GGU CCG UCU AAU G	Knocking-down			

Supplemental Table 5. Associations between selected SNP and CHD in two independent case-control studies

SNP	Group	Genotype	Control	Case	OR (95% CI) ^a	P ^b
rs11041321	Shanghai	CC	248 (77.3%)	238 (78.3%)	1.00	0.99
		CT	67 (20.9%)	60 (19.7%)	1.03 (0.68-1.58)	
		TT	6 (1.9%)	6 (2%)	1.03 (0.31-3.43)	
	Shandong	CC	465 (76.2%)	426 (75.5%)	1.00	0.95
		CT	138 (22.6%)	132 (23.4%)	0.99 (0.71-1.37)	
		TT	7 (1.1%)	6 (1.1%)	1.21 (0.36-4.08)	
rs153734	Shanghai	TT	186 (57.9%)	183 (60.2%)	1.00	0.58
		TC	114 (35.5%)	96 (31.6%)	0.95 (0.66-1.38)	
		CC	21 (6.5%)	25 (8.2%)	1.37 (0.71-2.68)	
	Shandong	TT	221 (36.2%)	219 (38.8%)	1.00	0.52
		TC	298 (48.9%)	275 (48.8%)	0.97 (0.72-1.30)	
		CC	91 (14.9%)	70 (12.4%)	0.78 (0.50-1.21)	
rs10986018	Shanghai	TT	316 (98.4%)	296 (97.4%)	1.00	0.46
		TC	5 (1.6%)	7 (2.3%)	1.65 (0.48-5.64)	
		CC	0 (0%)	1 (0.3%)	NA (0.00-NA)	
	Shandong	TT	607 (99.5%)	560 (99.3%)	1.00	0.078
		TC	2 (0.3%)	4 (0.7%)	8.47(0.88-81.09)	
		CC	1 (0.2%)	0 (0%)	0.00 (0.00-NA)	
rs199959	Shanghai	CC	115 (35.8%)	131 (43.1%)	1.00	0.07
		CT	167 (52%)	140 (46%)	0.65 (0.45-0.94)	
		TT	39 (12.2%)	33 (10.9%)	0.77 (0.43-1.36)	
	Shandong	CC	240 (39.3%)	242 (42.9%)	1.00	0.22
		CT	297 (48.7%)	265 (47%)	0.87 (0.65-1.17)	
		TT	73 (12%)	57 (10.1%)	0.66 (0.40-1.07)	
rs2119289	Shanghai	GG	195 (60.8%)	220 (72.4%)	1.00	0.0048
		GC	105 (32.7%)	74 (24.3%)	0.52 (0.35-0.78)	
		CC	21 (6.5%)	10 (3.3%)	0.36 (0.15-0.88)	
	Shandong	GG	359 (58.9%)	417 (73.9%)	1.00	0.0012
		GC	208 (34.1%)	134 (23.8%)	0.60 (0.44-0.82)	
		CC	43 (7%)	13 (2.3%)	0.23 (0.11-0.49)	
rs4654748	Shanghai	TT	115 (35.8%)	104 (34.2%)	1.00	0.76
		TC	160 (49.8%)	152 (50%)	1.15 (0.78-1.69)	
		CC	46 (14.3%)	48 (15.8%)	1.15 (0.67-1.97)	
	Shandong	TT	242 (39.7%)	222 (39.4%)	1.00	0.78
		TC	279 (45.7%)	266 (47.2%)	0.96 (0.71-1.29)	
		CC	89 (14.6%)	76 (13.5%)	0.86 (0.56-1.32)	

^a Adjusted for age and sex; ^bP value for the chi-square test and corrected by Bonferroni correction.

Supplemental Table 6. The maternal folic acid intake among different genotypes between cases and controls

Group	Maternal folic acid use		P value ^a	
	yes	no		
<i>Difference among genotypes</i>				
Control	GG	969	25	0.879
	GC	613	16	
	CC	118	4	
Case	GG	1,006	30	0.749
	GC	395	9	
	CC	48	1	
Control + Case	GG	1,975	55	0.867
	GC	1,008	25	
	CC	166	5	
<i>Difference between case & control</i>				
GG	Control	969	25	0.597
	Case	1,006	30	
GC	Control	613	16	0.747
	Case	395	9	
CC	Control	118	4	1.000
	Case	48	1	
GG/GC/CC	Control	1,700	45	0.849
	Case	1,449	40	

^aP value Significance was evaluated by the chi-square test.

Supplemental Table 7. Stratification analysis of rs2119289 genotypes according to CHD classifications and phenotypes

Variable	Case number	<i>P</i> value ^a	Association OR (95% CI) ^b	
CHD Classification			GC vs GG	CC vs GG
Septation defects	1,222	3.84×10⁻¹³	0.56 (0.47-0.67)	0.30 (0.20-0.46)
Conotruncal defects	267	0.0012	0.57 (0.40-0.79)	0.52 (0.27-1.02)
Detailed phenotype				
ASD (atrial septal defect)	193	9.55×10⁻⁶	0.47 (0.32-0.70)	0.18 (0.06-0.54)
VSD (ventricular septal defect)	932	1.92×10⁻⁸	0.61 (0.50-0.74)	0.30 (0.19-0.49)
TOF (tetralogy of Fallot)	210	0.039	0.64 (0.45-0.93)	0.64 (0.32-1.29)

The controls used were the total 1,745 combined controls. ^a*P* value in dominant genetic model; ^b Adjusted for age and sex.

Supplemental Table 8. The FIGN-interacting protein list (totally 165 proteins)

SN	Protein	Score	Coverage
1	Ig kappa chain V-II region MIL [KV203_HUMAN]	1241.40	14.29
2	CAD protein [PYR1_HUMAN]	294.50	4.54
3	Insulin receptor substrate 4 [IRS4_HUMAN]	251.97	9.63
4	RuvB-like 1 [RUVB1_HUMAN]	228.10	16.45
5	Tubulin beta-4A chain [TBB4A_HUMAN]	223.93	18.92
6	Heat shock protein HSP 90-alpha [HS90A_HUMAN]	214.04	8.33
7	ATPase family AAA domain-containing protein 3A [ATD3A_HUMAN]	205.30	12.93
8	RuvB-like 2 [RUVB2_HUMAN]	179.54	14.25
9	LanC-like protein 1 [LANC1_HUMAN]	166.45	12.53
10	Heterogeneous nuclear ribonucleoprotein A1 [ROA1_HUMAN]	161.37	12.90
11	Endoplasmic reticulum resident protein 44 [ERP44_HUMAN]	151.91	17.49
12	Myeloid leukemia factor 2 [MLF2_HUMAN]	151.75	15.73
13	Keratin, type I cytoskeletal 13 [K1C13_HUMAN]	138.03	7.86
14	ADP/ATP translocase 3 [ADT3_HUMAN]	135.29	20.13
15	Keratin, type I cuticular Ha3-II [KT33B_HUMAN]	131.63	8.91
16	Keratin, type I cuticular Ha1 [K1H1_HUMAN]	131.08	9.62
17	DnaJ homolog subfamily B member 6 [DNJB6_HUMAN]	126.44	10.74
18	ATPase family AAA domain-containing protein 3B [ATD3B_HUMAN]	124.28	7.87
19	26S protease regulatory subunit 8 [PSMC5_HUMAN]	121.18	7.39
20	Mitochondrial 2-oxoglutarate/malate carrier protein [M2OM_HUMAN]	120.63	5.10
21	Heat shock protein beta-1 [HSPB1_HUMAN]	119.82	17.07
22	F-box only protein 11 [FBX11_HUMAN]	118.02	3.88
23	Leucine-rich repeat flightless-interacting protein 1 [LRRF1_HUMAN]	117.31	3.84
24	ATP-dependent RNA helicase DDX3X [DDX3X_HUMAN]	115.25	4.98
25	DNA mismatch repair protein Msh2 [MSH2_HUMAN]	113.69	2.57
26	Peroxiredoxin-4 [PRDX4_HUMAN]	110.47	12.18
27	Elongation factor 1-gamma [EF1G_HUMAN]	110.03	5.26
28	T-complex protein 1 subunit zeta [TCPZ_HUMAN]	107.94	3.95
29	26S proteasome non-ATPase regulatory subunit 4 [PSMD4_HUMAN]	107.41	7.16
30	Tubulin alpha chain-like 3 [TBAL3_HUMAN]	103.32	5.38
31	Fatty acid synthase [FAS_HUMAN]	101.61	1.43
32	Junction plakoglobin [PLAK_HUMAN]	99.78	3.62
33	Pyruvate dehydrogenase E1 component subunit beta, mitochondrial [ODPB_HUMAN]	97.14	8.91
34	RING finger protein 219 [RN219_HUMAN]	95.27	6.47
35	Melanoma-associated antigen D1 [MAGD1_HUMAN]	95.26	6.56
36	BAG family molecular chaperone regulator 2 [BAG2_HUMAN]	95.12	9.48
37	Unconventional myosin-VI [MYO6_HUMAN]	93.96	2.47
38	PERQ amino acid-rich with GYF domain-containing protein 2 [PERQ2_HUMAN]	92.31	1.39
39	60S ribosomal protein L23 [RL23_HUMAN]	91.92	16.43
40	Translational activator GCN1 [GCN1L_HUMAN]	90.76	1.09
41	T-complex protein 1 subunit epsilon [TCPE_HUMAN]	89.31	1.85
42	Protein transport protein Sec23A [SC23A_HUMAN]	87.79	1.83

43	HLA class I histocompatibility antigen, B-7 alpha chain [1B07_HUMAN]	86.56	4.14
44	LIM domain and actin-binding protein 1 [LIMA1_HUMAN]	86.52	3.56
45	HCLS1-associated protein X-1 [HAX1_HUMAN]	86.16	15.41
46	Translocon-associated protein subunit gamma [SSRG_HUMAN]	84.86	7.57
47	Src substrate cortactin [SRC8_HUMAN]	83.22	4.55
48	Serine/threonine-protein phosphatase PGAM5, mitochondrial [PGAM5_HUMAN]	82.25	12.46
49	D-3-phosphoglycerate dehydrogenase [SERA_HUMAN]	81.60	4.32
50	MAX gene-associated protein [MGAP_HUMAN]	80.73	0.99
51	A-kinase anchor protein 8-like [AKP8L_HUMAN]	80.41	4.18
52	Nucleolin [NUCL_HUMAN]	79.84	2.96
53	Filamin-A [FLNA_HUMAN]	76.96	0.60
54	Clathrin heavy chain 1 [CLH1_HUMAN]	75.54	1.25
55	DnaJ homolog subfamily A member 1 [DNJA1_HUMAN]	74.27	5.29
56	S-adenosylmethionine synthase isoform type-2 [METK2_HUMAN]	73.57	3.80
57	Monocarboxylate transporter 1 [MOT1_HUMAN]	72.39	5.80
58	Prohibitin [PHB_HUMAN]	68.28	3.68
59	Apoptosis-inducing factor 1, mitochondrial [AIFM1_HUMAN]	68.25	4.89
60	Very-long-chain (3R)-3-hydroxyacyl-[acyl-carrier protein] dehydratase 3 [HACD3_HUMAN]	67.75	3.87
61	60S ribosomal protein L11 [RL11_HUMAN]	66.97	12.92
62	Ornithine aminotransferase, mitochondrial [OAT_HUMAN]	66.37	4.56
63	DNA replication licensing factor MCM7 [MCM7_HUMAN]	66.33	1.81
64	14-3-3 protein zeta/delta [1433Z_HUMAN]	65.11	8.98
65	28S ribosomal protein S7, mitochondrial [RT07_HUMAN]	65.04	4.55
66	Actin-related protein 2/3 complex subunit 2 [ARPC2_HUMAN]	64.41	7.67
67	Neutral amino acid transporter B(0) [AAAT_HUMAN]	63.59	3.88
68	Proteasome subunit alpha type-4 [PSMA4_HUMAN]	63.13	3.83
69	26S proteasome non-ATPase regulatory subunit 6 [PSMD6_HUMAN]	61.89	8.48
70	Lysophosphatidylcholine acyltransferase 1 [PCAT1_HUMAN]	60.91	2.81
71	Dolichyl-diphosphooligosaccharide--protein glycosyltransferase subunit 2 [RPN2_HUMAN]	60.84	1.90
72	26S proteasome non-ATPase regulatory subunit 2 [PSMD2_HUMAN]	59.93	4.19
73	E3 ubiquitin-protein ligase UBR5 [UBR5_HUMAN]	59.92	0.54
74	T-complex protein 1 subunit gamma [TCPG_HUMAN]	59.22	3.49
75	ADP-ribosylation factor-like protein 1 [ARL1_HUMAN]	58.49	8.84
76	ELAV-like protein 1 [ELAV1_HUMAN]	58.28	3.37
77	6-phosphofructokinase type C [K6PP_HUMAN]	57.71	1.53
78	Sarcoplasmic/endoplasmic reticulum calcium ATPase 2 [AT2A2_HUMAN]	57.66	1.15
79	Ubiquitin carboxyl-terminal hydrolase 15 [UBP15_HUMAN]	57.37	1.02
80	Heat shock protein 105 kDa [HS105_HUMAN]	56.05	1.28
81	DNA mismatch repair protein Msh6 [MSH6_HUMAN]	55.10	0.88
82	Delta(24)-sterol reductase [DHC24_HUMAN]	55.02	1.74
83	Interleukin enhancer-binding factor 2 [ILF2_HUMAN]	54.40	3.08
84	Polypyrimidine tract-binding protein 1 [PTBP1_HUMAN]	54.23	1.51
85	Gem-associated protein 4 [GEMI4_HUMAN]	53.93	1.04
86	ATP synthase subunit gamma, mitochondrial [ATPG_HUMAN]	53.48	7.05

87	Nuclease-sensitive element-binding protein 1 [YBOX1_HUMAN]	52.68	5.86
88	26S proteasome non-ATPase regulatory subunit 3 [PSMD3_HUMAN]	52.39	1.69
89	Unconventional myosin-Ic [MYO1C_HUMAN]	52.22	0.94
90	Small nuclear ribonucleoprotein F [RUXF_HUMAN]	51.75	13.95
91	Glutamate dehydrogenase 1, mitochondrial [DHE3_HUMAN]	51.75	2.87
92	Poly [ADP-ribose] polymerase 1 [PARP1_HUMAN]	51.61	1.28
93	Phenylalanine--tRNA ligase alpha subunit [SYFA_HUMAN]	51.51	2.17
94	NADH dehydrogenase [ubiquinone] 1 alpha subcomplex subunit 4 [NDUA4_HUMAN]	50.44	12.35
95	C-terminal-binding protein 1 [CTBP1_HUMAN]	50.20	2.05
96	Protein transport protein Sec61 subunit alpha isoform 1 [S61A1_HUMAN]	49.73	2.31
97	Keratin, type II cuticular Hb2 [KRT82_HUMAN]	49.41	3.70
98	Matrin-3 [MATR3_HUMAN]	49.30	4.60
99	Dedicator of cytokinesis protein 7 [DOCK7_HUMAN]	48.87	1.64
100	Splicing factor 3B subunit 4 [SF3B4_HUMAN]	47.97	3.07
101	Far upstream element-binding protein 2 [FUBP2_HUMAN]	47.17	1.55
102	Ig kappa chain V-III region CLL [KV308_HUMAN]	46.93	19.38
103	Delta-1-pyrroline-5-carboxylate synthase [P5CS_HUMAN]	46.87	1.51
104	Nuclear receptor subfamily 2 group F member 6 [NR2F6_HUMAN]	46.30	1.98
105	Histone deacetylase 1 [HDAC1_HUMAN]	45.73	2.49
106	PEST proteolytic signal-containing nuclear protein [PCNP_HUMAN]	45.44	8.43
107	Serine palmitoyltransferase 1 [SPTC1_HUMAN]	43.92	2.96
108	RNA-binding motif protein, X chromosome [RBMX_HUMAN]	43.88	5.37
109	Pyrroline-5-carboxylate reductase 2 [P5CR2_HUMAN]	42.35	5.31
110	Stomatin-like protein 2, mitochondrial [STML2_HUMAN]	42.33	4.21
111	Serum amyloid P-component [SAMP_HUMAN]	42.18	2.69
112	YTH domain-containing family protein 2 [YTHD2_HUMAN]	42.16	2.07
113	Influenza virus NS1A-binding protein [NS1BP_HUMAN]	40.87	2.02
114	Dolichol-phosphate mannosyltransferase subunit 1 [DPM1_HUMAN]	40.36	4.23
115	Fatty acyl-CoA reductase 1 [FACR1_HUMAN]	40.27	3.69
116	MARCKS-related protein [MRP_HUMAN]	39.14	7.69
117	Cytochrome b-c1 complex subunit 2, mitochondrial [QCR2_HUMAN]	39.05	3.53
118	Protein TXNRD3NB [TR3N_HUMAN]	38.72	4.51
119	Exportin-1 [XPO1_HUMAN]	38.51	1.96
120	Calmodulin-like protein 3 [CALL3_HUMAN]	37.62	5.37
121	Polyadenylate-binding protein 3 [PABP3_HUMAN]	37.45	1.58
122	Leucine-rich PPR motif-containing protein, mitochondrial [LPPRC_HUMAN]	37.38	0.79
123	E3 ubiquitin-protein ligase TRIM21 [RO52_HUMAN]	37.05	6.74
124	Heterogeneous nuclear ribonucleoprotein D0 [HNRPD_HUMAN]	36.35	3.94
125	X-ray repair cross-complementing protein 6 [XRCC6_HUMAN]	36.35	1.31
126	26S protease regulatory subunit 6A [PSMC3_HUMAN]	36.30	7.29
127	Monofunctional C1-tetrahydrofolate synthase, mitochondrial [C1TM_HUMAN]	36.00	2.86
128	Very-long-chain enoyl-CoA reductase [TECR_HUMAN]	34.78	3.25
129	Ribose-phosphate pyrophosphokinase 3 [PRPS3_HUMAN]	34.74	4.09
130	T-complex protein 1 subunit alpha [TCPA_HUMAN]	34.71	2.70

131	Haptoglobin [HPT_HUMAN]	34.12	2.22
132	Guanine nucleotide-binding protein subunit beta-2-like 1 [GBLP_HUMAN]	33.51	3.15
133	Far upstream element-binding protein 3 [FUBP3_HUMAN]	32.45	2.45
134	Pre-mRNA-processing factor 6 [PRP6_HUMAN]	32.07	1.06
135	NADH dehydrogenase [ubiquinone] 1 alpha subcomplex subunit 13 [NDUAD_HUMAN]	31.95	9.03
136	KH domain-containing, RNA-binding, signal transduction-associated protein 1 [KHDR1_HUMAN]	31.86	3.16
137	Prohibitin-2 [PHB2_HUMAN]	31.63	3.68
138	Pinin [PININ_HUMAN]	31.25	1.26
139	Dolichyl-diphosphooligosaccharide-protein glycosyltransferase 48 kDa subunit [OST48_HUMAN]	31.14	1.97
140	Maternal embryonic leucine zipper kinase [MELK_HUMAN]	30.47	2.61
141	Lamina-associated polypeptide 2, isoforms beta/gamma [LAP2B_HUMAN]	30.26	3.52
142	60S ribosomal protein L36a [RL36A_HUMAN]	30.04	7.55
143	Emerin [EMD_HUMAN]	29.70	3.15
144	BAG family molecular chaperone regulator 3 [BAG3_HUMAN]	29.63	1.57
145	Ribosome biogenesis protein BMS1 homolog [BMS1_HUMAN]	28.99	0.94
146	26S proteasome non-ATPase regulatory subunit 13 [PSMD13_HUMAN]	28.53	4.79
147	Nuclear pore glycoprotein p62 [NUP62_HUMAN]	28.10	2.68
148	Pyruvate dehydrogenase E1 component subunit alpha, mitochondrial [ODPA_HUMAN]	27.91	3.33
149	DnaJ homolog subfamily A member 2 [DNJA2_HUMAN]	27.18	1.94
150	6-phosphofructokinase, muscle type [K6PF_HUMAN]	27.08	1.41
151	39S ribosomal protein L2, mitochondrial [RM02_HUMAN]	26.40	1.97
152	Choline transporter-like protein 3 [CTL3_HUMAN]	26.22	2.60
153	Poly(rC)-binding protein 2 [PCBP2_HUMAN]	25.80	3.56
154	T-complex protein 1 subunit beta [TCPB_HUMAN]	25.49	2.06
155	Calnexin [CALX_HUMAN]	25.27	3.21
156	Protein transport protein Sec24C [SC24C_HUMAN]	24.13	1.37
157	DnaJ homolog subfamily A member 3, mitochondrial [DNJA3_HUMAN]	23.98	2.50
158	ATP-dependent RNA helicase DDX39A [DX39A_HUMAN]	22.40	2.34
159	39S ribosomal protein L12, mitochondrial [RM12_HUMAN]	21.83	5.05
160	Zinc finger and BTB domain-containing protein 24 [ZBT24_HUMAN]	21.66	0.86
161	Complement component 1 Q subcomponent-binding protein [C1QBP_HUMAN]	0.00	7.09
162	Probable ATP-dependent RNA helicase DDX46 [DDX46_HUMAN]	0.00	1.07
163	Pre-mRNA branch site protein p14 [PM14_HUMAN]	0.00	11.20
164	60S ribosomal protein L32 [RL32_HUMAN]	0.00	5.93
165	Splicing factor U2AF 26 kDa subunit [U2AF4_HUMAN]	0.00	5.45

Supplemental Table 9. FIGN interacts with proteasome subunits

Protein	Score	Coverage	Peptides	MW (kDa)
26S protease regulatory subunit 8 (PSMC5)	121.2	7.4	2	45.6
26S proteasome non-ATPase regulatory subunit 4 (PSMD4)	107.4	7.2	2	40.7
Proteasome subunit alpha type-4 (PSMA4)	63.1	3.8	1	29.5
26S proteasome non-ATPase regulatory subunit 6 (PSMD6)	61.9	8.5	3	45.5
26S proteasome non-ATPase regulatory subunit 2 (PSMD2)	60.0	4.2	2	100.1
26S proteasome non-ATPase regulatory subunit 3 (PSMD3)	52.4	1.7	1	60.9
26S protease regulatory subunit 6A (PSMC3)	36.3	7.3	2	49.2
26S proteasome non-ATPase regulatory subunit 13 (PSMD13)	28.5	4.8	1	42.9

Supplemental Figure 1. Annotation of *FIGN* regulatory sequences in intron 4 and promoter regions.

(a) The region around rs2119289 in intron 4 is an alternative promoter for *FIGN* isoform X3 transcription. The C allele of rs2119289 destroys the binding site of CREB1 to the new promoter. (b) CREB1 has not binding site in the *FIGN* promoter.

a

FIGN intron 4

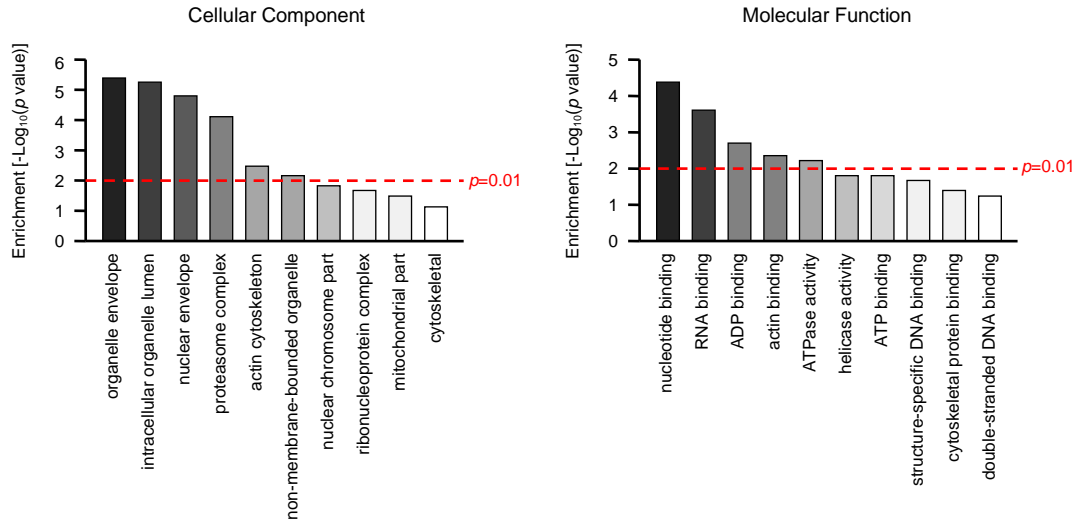


b

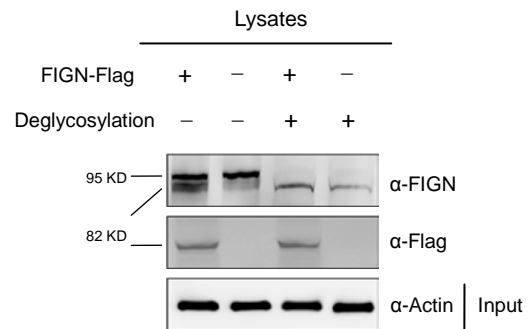
FIGN promoter



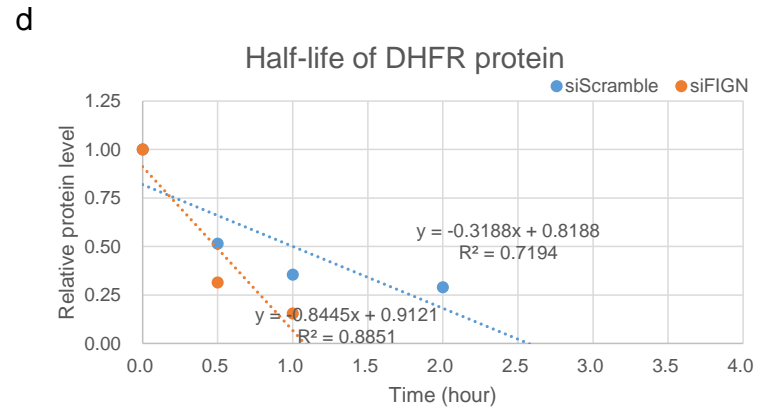
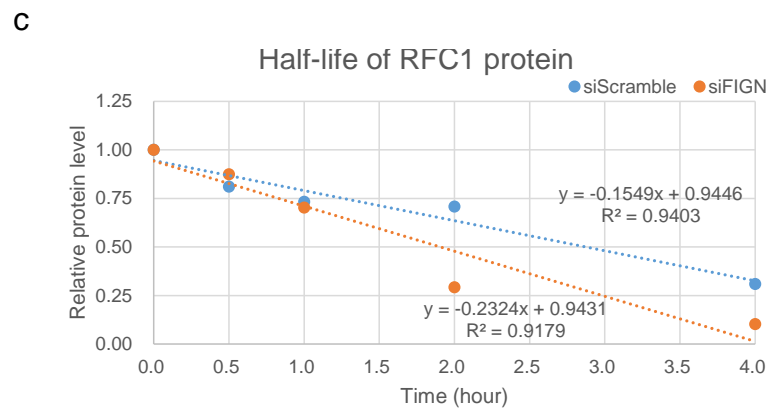
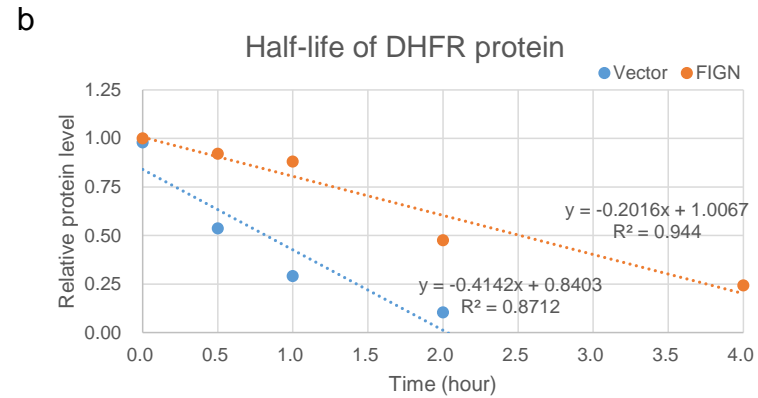
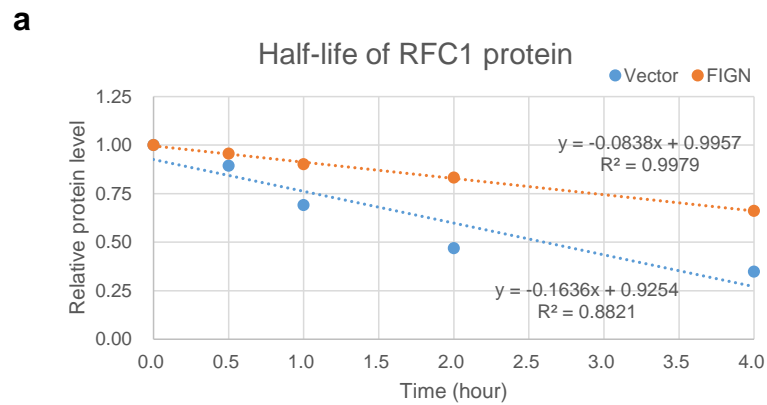
Supplemental Figure 2. Cellular component and molecular function analysis on FIGN-interacting proteins identified by proteomic survey using tandem affinity purification.



Supplemental Figure 3. Endogenous FIGN was glycosylated. The predicted band size of FIGN in western blotting was 82 kDa. The observed band size of endogenous and exogenous FIGN were 95 kDa and 82 kDa, respectively. When we deglycosylated FIGN *in vitro* using protein deglycosylation kit (NEB P6039S), the endogenous FIGN showed the same size with predicted molecular weight.



Supplemental Figure 4. Half-lives calculations of RFC1 and DHFR proteins in CHX treated HEK293T cells transfected with either *FIGN* or empty vector, or siRNA targeting *FIGN* or scramble sequence. The half-lives values were listed below: a) RFC1 in vector overexpression was 2.6 h, in *FIGN* overexpression was 5.9 h; b) DHFR in vector overexpression was 0.8 h, in *FIGN* overexpression was 2.5 h; c) RFC1 in siScramble was 2.9 h, in si*FIGN* was 1.9 h; d) DHFR in siScramble was 1 h, in si*FIGN* was 0.5 h.



Supplemental Reference

1. Zhao JY, Yang XY, Shi KH, Sun SN, Hou J, Ye ZZ, Wang J, Duan WY, Qiao B, Chen YJ, Shen HB, Huang GY, Jin L, Wang HY. A functional variant in the cystathionine β -synthase gene promoter significantly reduces congenital heart disease susceptibility in a Han Chinese population. *Cell Res.* 2013; 23:242-253.